Technion Research & Development Foundation

Summary report on project 2025039

Methodology and devices for safe flutter tests

Sponsored by Civil Aviation Authority of Israel (CAAI), Ministry of Transport

This research was done in collaboration with ASSURE[1] program

Principal Investigator:

Prof. Emeritus Moti Karpel
Technion – Israel Institute of Technology

February 2021

[1] The FAA's Center of Excellence for UAS Research. ASSURE – Alliance for System Safety of UAS through Research Excellence.

Notice

This document is disseminated under the sponsorship of the Civil Aviation Authority of Israel (CAAI), Ministry of Transport in the interest of information exchange.

The Government of Israel assumes no liability for the contents or use thereof.

The findings and conclusions in this report are those of the author(s) and do not necessarily represent the views of the funding authority.

This document does not constitute CAAI policy.

Executive Summary

The safe-flutter-test research project was intended to be one of 4 research programs to be carried out by the ASSURE consortium of US universities and the Faculty of Aerospace Engineering at Technion, supported by the US Federal Aviation Administration (FAA) and the Civil Aviation Authority of Israel (CAAI). The final proposal of the current research was submitted to MOT/CAAI in August 2017, after conducting initial discussions with a test group at Ohio State University (OSU), a member of the ASSURE program. The proposed plan included 4 parts:

1. Method advancement: (a) further development of the PFM methodology, simulation tools and application models; (b) an additional 3D test to be performed at Technion; and (c) summary of the related wind-tunnel tests. (6 months)
2. Flight test planning: Simulations to investigate the intended system performance with a generic UAV model and available shakers in collaboration with the ASSURE partner. (6 month)
3. Flutter tests and data reduction to be performed mainly by the ASSURE partner. (6 months)
4. Impact on flutter test procedures regulations: exploration of ways to improve the flight-test procedures in terms of safety, duration and cost. (6 months)

The first year of the proposed research (Items 1 and 2 above), has been performed successfully and exhibited very promising results. However, since OSU participation has not been formally approved and financed yet by FAA, the data obtained from them was limited to conceptual design data the UAV wing.

The second year of the program started with selecting a proper shaking device and its mounting location. An existing shaker/accelerometer device of about 70 gr seems to be suitable for the task when located at a front location in the wing-tip store. An additional device of about 200 gr, with a battery, driver circuit and reference accelerometer, may also be added at another location where it has small effect of critical flutter characteristics. When it became clear that OSU are not going to start their project soon, we changed our test-case model to be the Active Aeroelastic aircraft TestBed (A3TB) vehicle developed at Technion by Prof. Raveh as a student project. This UAV is currently at its preliminary flight test stage and it was designed such that it supposed to meet flutters in it flight envelope.

The PFM flutter analysis method, on which the planned flutter tests of our project are based, was expanded to accommodate a sensitivity study for flutter characteristics vs. added mass magnitude and location. Such sensitivity study with the A3TB vehicle showed that the original flutter velocity of about 24 m/s can be changed to about 34 m/s with 300gr mass added at the leading edge of the wing-tip sections. Both velocities are inside the flight envelope, so this case may become an excellent experimental testcase for the safe flutter test methodology.

The PFM method was further expanded to accommodate a simulation of experimental noise generated by air turbulence. It was shown that the combination of the aircraft response to intentional excitation by a shaker, at the point of added mass, with turbulence noise, may still provide adequate measurement signals for the extraction of flutter margins with which the test may proceed safely.

Table of Contents

1 Introduction

The main purpose of the safe flutter test project is to develop a procedure and means for conducting safer and more efficient UAV flutter flight tests, such as those required by the aviation regulations FAR 25.629 and USAR 629. Ultimately, the research goal is to yield a major reduction of the associated risk, time duration and costs. Furthermore, it may lead to improved criteria and equipment to be used in UAV airworthiness certification programs. The research is based on the recently developed numerical Parametric Flutter Margin (PFM) method [1] that calculates flutter margins and LCO levels, based on frequency-response functions calculated with stabilizing elements added to the structure or the control system.

In its initial version, the PFM method is based on adding a single stabilizing parameter, such as a certain modal damping coefficient or a discrete mass, which increases the flutter stability margins. This version facilitated very efficient massive sensitivity studies with respect to selected stabilizing parameters [2]. Furthermore, it facilitated safer flutter tests where flutter or nonlinear limit-cycle oscillation (LCO) boundaries of a certain configuration are positively identified while actually testing a more stable configuration. This idea was first presented at Israeli IACAS 2017 conference [3] and formed the basis for our preliminary proposal submitted to CAAI and the ASSURE consortium in January 2017. The first proof-of-concept wind-tunnel test with a 2D model was performed at TUDelft in April 2017 [4]. The Technion team directed the test plan, participated in the 5-day test and processed the test results.

A 3D wind-tunnel test was performed at Technion, with an existing model that was slightly modified for the PFM test [5]. The results of the two wind-tunnel tests in Refs. [4, 5] were reviewed and investing, and the PFM method was adapted to the specific parameters of the intended flight tests in the first part of the 1st year. The second part of the 1st-year research was intended to include preliminary design and analysis of a flight-test vehicle, and an initial plan for the ground and flight tests, to be done at OSU. However, since the official collaboration started only in October 2020, the OSU part was limited to the conceptual geometrical design of the wing only. Technion’s part was shifted towards basic normal-modes and flutter analyses, conceptual design of the flight-test devices and preliminary ideal test simulations.

The delay in starting the OSU part of the project caused changes in the plans for the 2nd year of the project. While some exchange of ideas regarding the intended shakers continued, the main method development activities were modified to prepare advanced tools for the detailed-design and flight-test stages that are expected in the project-continuation plan. A significant delay was caused by the Corona-virus crisis, which caused the end of the 2-year program to be postponed by more than 6 months, until end of March 2021, with no change in the funding. The simulation tools were applied in the 2nd year mainly to the Technion's Active Aeroelastic Testbed (A3TB) UAV [6], in preparation for the flight tests expected in the autumn of 2021. This research is applicable to all types of fixed-wing air vehicle.

2 PFM method advancement

2.1 Generalized parametric flutter margin (PFM) method

Linear ASE dynamic stability analysis techniques are aimed at finding the flight conditions that define the flutter boundary, at which there is a nontrivial solution to the homogeneous aeroelastic frequency-domain (FD) equation of motion,

$$\left[A(i\omega)\right]\left\{x_L(i\omega)\right\} = \left\{0\right\} \tag{1}$$

where $\{x_L(i\omega)\}$ is the FD vector of modal displacements, linear control-system states and actuator states, $\left[A(i\omega)\right]$ is the closed-loop linear system matrix that includes the structural inertial, viscous and stiffness effects, the aerodynamic effects and the control-system ones. While common flutter solutions are based on finding the conditions at which $\left|A(i\omega)\right| = (0.,0.)$, the Parametric Flutter Margin (PFM) method is based on FRFs with a stabilizing flutter parameter, p_f, added to the ASE system. Flutter margins are defined by the factored value of p_f that would cause flutter if removed from the modified system. At the flutter boundary, this factor would be 1.0.

The PFM method was first presented in [1] in its single-input-single-output (SISO) version, in which the selected p_f must be such that its effects can be removed by a SISO control feedback. In this report, we first deal with the more general multi-input-multi-output (MIMO) PFM version [2]. The combination of flutter onset velocity V_f, the associated flutter frequency ω_f and the respective flutter mode $\left\{x_f(i\omega_f)\right\}$ that solves Eq. (1) characterizes the flutter boundary. The only constraint on p_f is that it must be defined such that its effect on the FD equation of motion can be expressed by

$$\begin{aligned}&\left[A(i\omega) + P_f B(i\omega)C(i\omega)\right]\left\{x(i\omega)\right\} = \left[B(i\omega)\right]\left\{u(i\omega)\right\}\\&\left\{y(i\omega)\right\} = \left[C(i\omega)\right]\left\{x(i\omega)\right\}\end{aligned} \tag{2}$$

where the input and output vectors are of the same size. It may be observed that the point (V,ω) at which there is an input vector $\left\{u_f(i\omega)\right\}$ that yields the output $\left\{y_f(i\omega)\right\}$ that satisfies

$$\left\{y_f(i\omega)\right\} = \left\{u_f(i\omega)\right\} / P_f \tag{3}$$

must be a flutter onset point, (V_f, ω_f). One may deduce this statement from the fact that Eqs. (3) and (2) yield Eq. (1). The solution $\left\{x_f(i\omega)\right\}$ of Eq. (2) forms in this case a nontrivial solution to Eq. (1), which is the flutter mode. Eqs. (2) and (3), with the real-valued P_f in Eq. (3) replaced by $1/\lambda\left(i\omega\right)$, yield the eigenvalue problem

$$\left[T(i\omega)\right]\left\{u(i\omega)\right\} = \lambda(i\omega)\left\{u(i\omega)\right\} \tag{4}$$

where $$\left[T(i\omega)\right] = \left[C(i\omega)\right]\left[A(i\omega) + P_f B(i\omega) C(i\omega)\right]^{-1}\left[B(i\omega)\right].$$

The numerical process for finding a flutter onset point is:

1. Define ranges of V and ω, and their increments.
2. For each velocity, solve Eq. (4) for the eigenvalues $\lambda_i(i\omega)$.
3. Plot the magnitude $G_i(\omega)$ and phase $\phi_i(\omega)$ of $\lambda_i(i\omega) * p_f$.
4. Interpolate for $G_i(\omega_{pco})$ where ω_{pco} is the phase-cross-over frequency at which $\phi_i(\omega_{pco}) = 0$. The system is stable when all $G_i(\omega_{pco}) < 1.0$.
5. Plot the gain $G_i(\omega_{pco})$ and the frequency ω_{pco} vs. V.
6. Interpolate for V_f, at which $G_i(\omega_{pco}) = 1.0$ and extract $\omega_f = \omega_{pco}$.
7. Solve for the flutter mode $\left\{x_f(i\omega)\right\}$ of Eq. (11) at (V_f, ω_f).

Flutter margins can be defined in two ways. The first one is by the gain $G_i(\omega_{pco})$, in [dB],

$$PFM = -20\log\left(G_i(\omega_{pco})\right)[dB] \tag{5}$$

that becomes 0dB when $G_i(\omega_{pco}) = 1.0$. The second way is by the increment ΔP_f that would bring the system to the flutter boundary

$$\Delta P_f = P_f - 1/\lambda\left(\omega_{pco}\right)_{\max} \tag{6}$$

Unlike Equation (5), Eq. (6) can be applied with $P_f = 0$, which implies that the eigenvalue analyses associated with different design parameters may be based on the same decomposition of the system matrix inversion $\left[A(i\omega)\right]$. This may be very helpful in design optimization with structural and control variables.

As discussed below, the simplified SISO version of the PFM method may be more efficient in flutter and LCO analyses, various sensitivity studies and flutter tests. The MIMO approach, however, may be of greater value in sensitivity analysis with respect to actual design variables. Reference [2] presents a flutter perturbation study with respect to a factor

P_f that multiplies the mass matrix of a refuelling pod mounted near the GTA wing's tip. A single MIMO-PFM analysis is shown in [2] to provide the variations in the flutter characteristics for several flutter mechanisms over a selected velocity range. The results are show in [2] to be practically identical to those obtained from numerous MSC/NASTRAN flutter runs.

Another application of the MIMO-PFM method in [2] is for calculating classic "V-g plots" of the variations of aeroelastic frequency and damping vs. velocity, which may be very instrumental in certification documents and in comparing PFM results with classic ones. This is done by defining P_f as a structural damping coefficient. With the modal displacements in $\{x(i\omega)\}$ used as "sensors", and the distribution matrices in Eq. (2) being $[B_f(i\omega)]=[I]$ and $[C_f(i\omega)]=i[K_{hh}]$, $\left[A(i\omega)\right]$ is supplemented with an extra modal damping matrix $ip_f[K_{hh}]$. The resulting ΔP_f of Eq. (6) is the damping coefficient g needed to be added to the nominal system for making it neutrally stable, which agrees with the classic *V-g*-plot concept. Figure 1 compares the MIMO-PFM results with those obtained with the commonly used *p-k* method. The same flutter point (at g=0) is obtained in both methods and the curve variations are similar. There are slight differences between the damping curves because the added g-related damping term in NASTRAN's *p-k* application [7] involves the aerodynamic matrix as well.

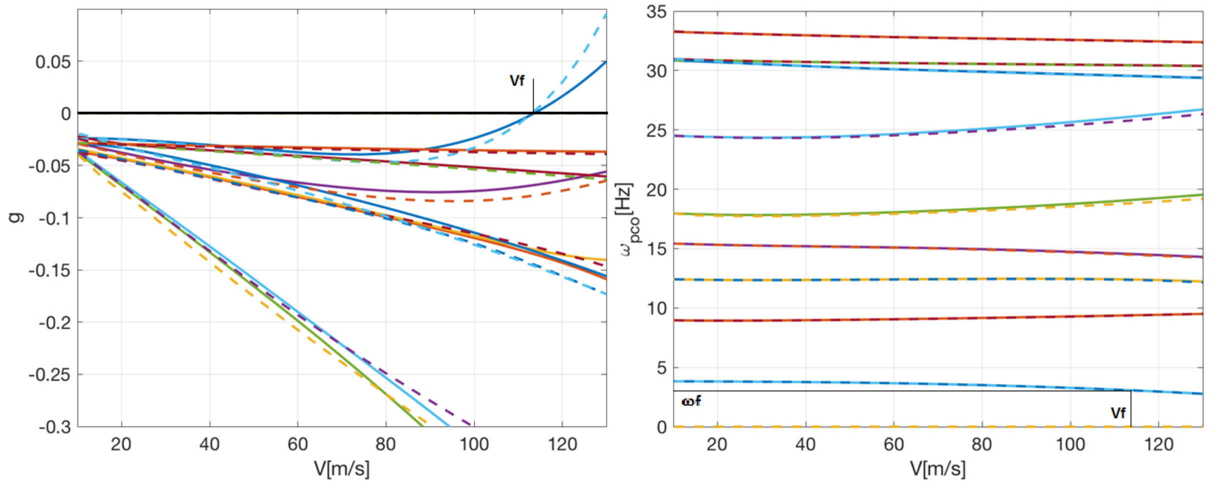

Figure 1: *V-g* plots computed by MIMO-PFM (solid) and *p-k* (dashed), taken from [2]

2.2 Linear SISO-PFM method

When the flutter parameter is limited to those that can be expresses by SISO feedback loops, the incremental $\left[P_f\left\{B(i\omega)\right\}\left\lfloor C(i\omega)\right\rfloor\right]$ matrix in Eq. (2) is now of rank1. This facilitates a solution that is based on SISO dynamic response functions without resorting to eigenvalue analysis. Another important application of the SISO-PFM scheme is in performing safe flutter tests, as discussed in the following chapters.

The input and output vectors in Eq. (2) become scalars in the SISO-PFM formulation,

$$\begin{aligned}&\left[\bar{A}_v(i\omega)+B_f P_f C_f\ (i\omega)\right]\left\{x_v(i\omega)\right\}=\left\{B_f\right\}u_f(i\omega)\\&y_f(i\omega)=\left\lfloor C_f\ (i\omega)\right\rfloor\left\{x_v(i\omega)\right\}\end{aligned}\tag{7}$$

Where $\left[\bar{A}_v(i\omega)\right]$ is the original system matrix with all its actual control loops closed, when applicable. It is easy to see that if the open control loop in Eq. (7) is closed by the SISO gain P_f, such that

$$u_f\left(i\omega\right)=P_f y_f\left(i\omega\right)\tag{8}$$

we get the homogeneous equation

$$\left[\bar{A}_v(i\omega)\right]\left\{x_v(i\omega)\right\}=\left\{0\right\}\tag{9}$$

that yields a non-trivial solution at the flutter boundary when $\left|\bar{A}_v(i\omega)\right|=0$. This implies that the interpolated velocity-frequency pair, for which Eq. (8) is satisfied, forms the flutter velocity V_f and the flutter frequency ω_f.

The selected P_f, and the associated single output and single input parameters of Eq. (7), yield frequency response functions to sinusoidal inputs of amplitude $u_f(i\omega)=1.0$. The FRFs may presented as Bode plots by their gain and phase variations with frequency

$$G(\omega)=20\log\left|P_f y_f(i\omega)\right|[dB];\quad \Phi(\omega)=\angle\left(P_f y_f(i\omega)\right)[\deg]\tag{10}$$

The original PFM method [1] used these gain and phase expressions as a basis for calculating flutter gain margins. The Bode plots are generated for selected points along a line in the flight envelop. The points can be of various air velocities at constant altitude, and various altitudes along a constant Mach line. In a search for non-match flutter conditions at constant altitude and Mach number, the phase function at each flight velocity is used for finding the associated phase-crossover frequencies ω_{co} at which $\Phi(\omega_{co})=\pm 360^o n$. The gains at these frequencies form the parametric flutter margins

$PFM = -G(\omega_{pco})$. The velocity and phase-crossover frequency for which PFM=0dB are V_f and ω_f. The associated solution of Eq. (2) is the flutter mode $\left\{x_f(i\omega)\right\}$.

The Dynresp framework provides for using a selected ASE response parameter, y_f, which can be defined as a frequency-dependent linear combination of the system states and control inputs, as a "sensor". When the selected P_f is an actual control gain, the stability analysis in Dynresp provides the standard Nyquist SISO control gain and phase margins [8], with aeroelastic effects of course.

An alternative flutter margin, which may be more useful in flutter tests, is defined as the incremental flutter parameter ΔP_f that, if added to the nominal system, would bring it to the verge of flutter. This definition implies

$$\left(P_f - \Delta P_f\right) y_f(\omega_{co}) / u_f(\omega_{co}) = 1 \quad \Rightarrow \quad \Delta P_f = P_f - u_f(\omega_{co}) / y_f(\omega_{co}) \tag{11}$$

where $u_f(\omega_{co})$ is not necessarily (1., 0.), to accommodate arbitrary input amplitude and phase in the test.

An example of added flutter parameter P_f that can be practically used in the planned flutter flight tests is a concentrated mass located at a "good" place that increases the flutter velocity. It is assumed here that the mass effect of flutter is significant only in one direction, i.e. normal to the lifting surface. An excitation u_f force is applied applied at this location and a co-located acceleration measurement y_f is taken, both in the effective direction. The PFM method is applied with these parameters, at selected flight velocities, to find ω_{co} and calculate the increment ΔP_f of Eq. (11). This increment is now the added mass Δm that would cause flutter at the selected flight velocity. At flight conditions where $\Delta m < P_f$, the tested configuration is stable. However, the removal of $P_f - \Delta m$ would make it unstable. In this way, by testing a stable configuration, we can positively map the unstable regions of other configurations.

2.3 PFM Wind-Tunnel Flutter Tests

The applicability of the PFM method for performing safe-flutter tests was demonstrated in two wind-tunnel tests performed in preparation for the current project. The first one [4] was performed on a 2D-proof-of-concept airfoil, where a simple wing section mounted on heave and pitch springs was tested (see Fig. 2). Motion stoppers allowed direct measurement of the flutter onset conditions by increasing the air velocity until flutter was observed. These conditions were then found by PFM, where a mass forward the elastic axis stabilized the system, and FRFs were generated by hammer hits. A load cell and an accelerometer added to the mass were used for measuring the excitation force $u_f(t)$ and mass acceleration $y_f(t)$. Using Fast Fourier Transform (FFT) the time signals were transformed to FD, and Bode plots of Eq. (10) were generated with the stabilizing mass as P_f.

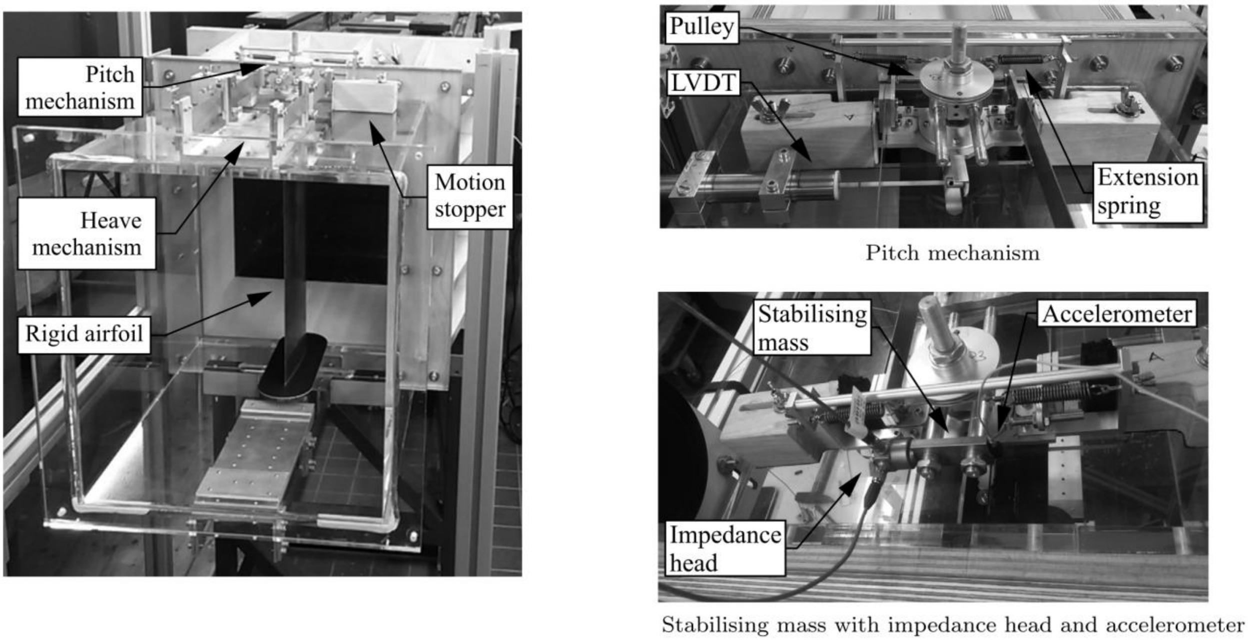

Figure 2: First wind-tunnel PFM-flutter test set up taken from [4].

The flutter-onset conditions obtained by the direct-flutter approach were V_f=22.7m/s and ω_f=5.08Hz. Figure 3 shows three Bode plots obtained at 22m/s, 23m/s and 24.2m/s. It is clear that flutter is identified near 23m/s at about ω_{pco}=5.1Hz, very close to the actual flutter conditions.

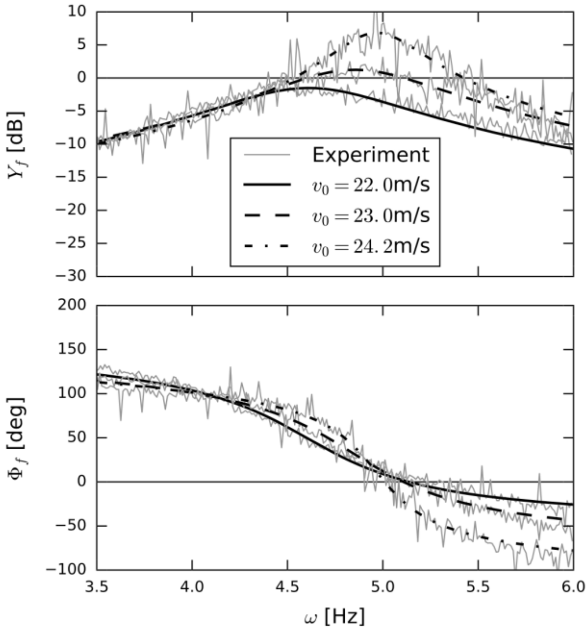

Figure 3: PFM Bode plots [4].

The second PFM-flutter test used a more realistic 3D aeroelastic wind-tunnel model experiencing bending-torsion flutter [5]. The flexible clamped wing model is shown in Fig. 4. The test is like the one in Ref. [4] in the sense that a mass located at the wing tip forward the elastic axis was used for stabilizing the system. The major differences between the tests (besides the model) is the excitation force and measurement equipment: while in Ref. [4] the force and acceleration at the mass location were measured, in Ref. [5] they were estimated from sensors at other locations.

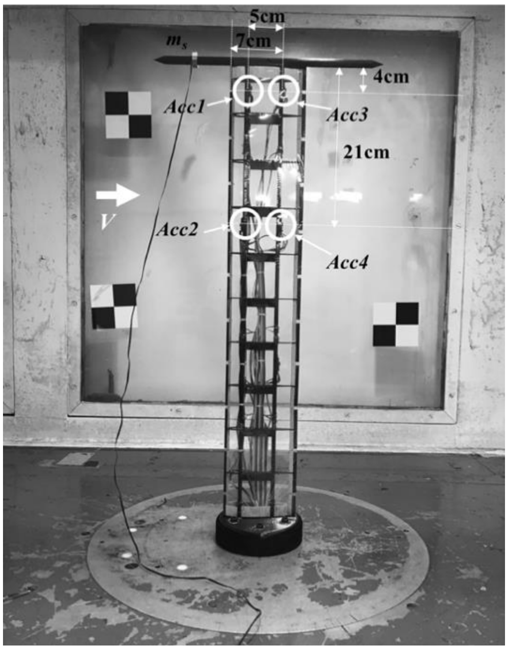

Figure 4: Elastic wing mounted in the wind tunnel, and location of the mass and accelerometers; taken from [5].

The flutter-onset conditions obtained by performing risky direct flutter test were 39.8m/s and 13.2Hz. Figure 5 shows typical Bode plots of Eq. (10), and a moving average filter for smoothing the experimental data, for three different velocities, 38.2, 39.4 and 40.4m/s. The span of the moving average filter is five. These velocities are shown because, as indicated by the cross-over frequencies, ω_{pco}, and the related *FM* values, the first curve (blue) indicates a positive flutter margin for the nominal system, the second one (red) indicates an almost zero margin, and the third one (black) exhibits a negative margin. Each curve has more than one phase-cross-over frequency in the frequency range of [3,20]Hz, but only the ones with lower *FM* need to be considered for calculating the flutter conditions. In spite of the scattered results due to the aerodynamic noise, it is clear that the system is stable at 38.2m/s and unstable at 40.4m/s. It can be observed that, while the moving average filter smooths the Bode plots, the cross-over points are not significantly affected.

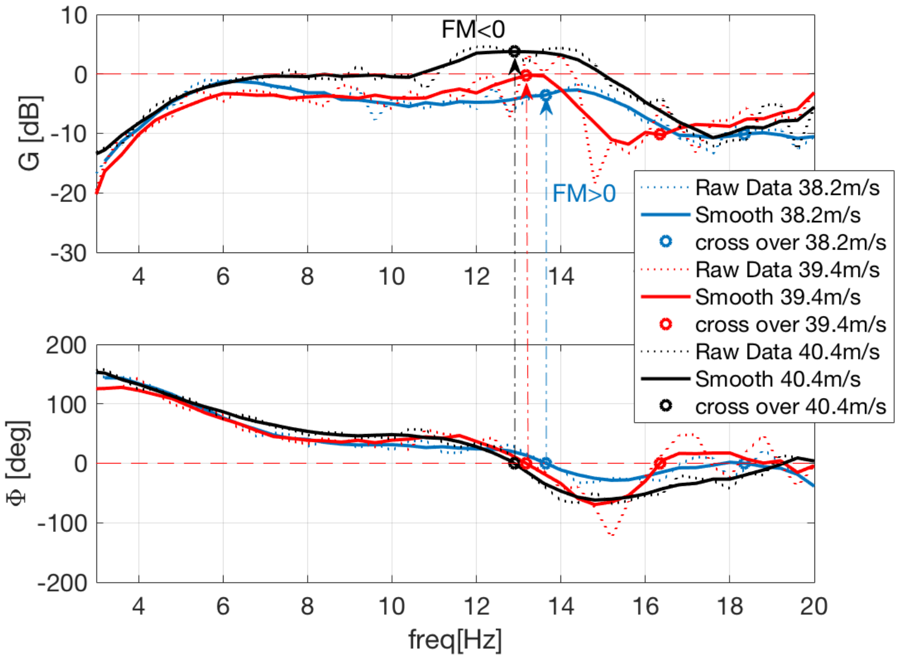

Figure 5: Experimental Bode plots for *V*=38.2, 39.4 and 40.4m/s [5].

3. Conceptual design and flutter analysis of OSU vehicle

3.1 Conceptual design

The design concepts were discussed in a preliminary meeting held with Prof. Jim Gregory and Dr. Matt McCreenk of Ohio State University (OSU) at Technion, December 2018, at the SciTech conference in January 2020 and in Zoom meetings since. OSU has a UAV with single electric engine to which they are going to replace the wing with a 3.3*m*-span flexible one. It is planned to be a straight wing with two uniform spars on which 3D-printed segments, wrapped by a transparent skin will be mounted. The rest of the aircraft assumed rigid at this point.

A general view of the planned test vehicle is given in Figure 6. Each wing will be constructed with 8 segments. There will be two types of segments shown in Figure 7. Six of the segments will be without ailerons and 2 (No. 6 and 7 from the root) with ailerons. The two aileron segments will be interconnected and driven by a single actuator. The tip pod will be designed to carry dummy masses that will cause the nominal flutter velocity to be in the flight envelop. Shakers placed in a forward point of each tip pod will move the flutter velocity up and provide the excitation needed for identifying the nominal flutter velocity using the PFM method.

Figure 6: General view of the test vehicle

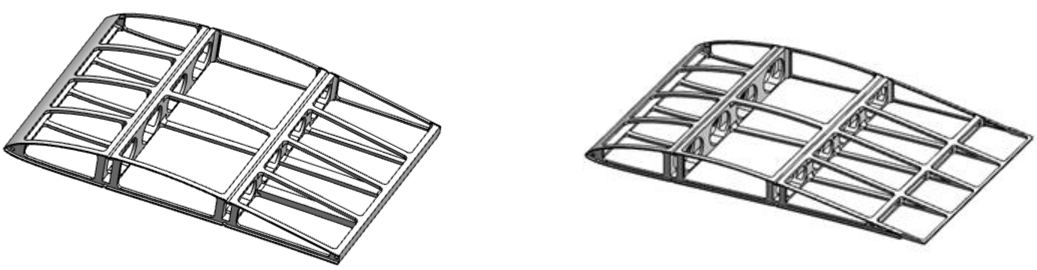

Figure 7: Two types of segments: without (left) and with (right) aileron.

Parasolid CAD files for the two types of wing sections were obtained from OSU. The one with the aileron (Wing_Profile_RP_Aileron.x_t) is shown in Fig. 8. The chord length is 0.33m and the segment span is 0.2057m. The local segment coordinate system is rotated about the X axis with respect to the main one of the finite-element model (FEM) below. A similar file was created for a segment without aileron (Wing_Profile_RP.x_t).

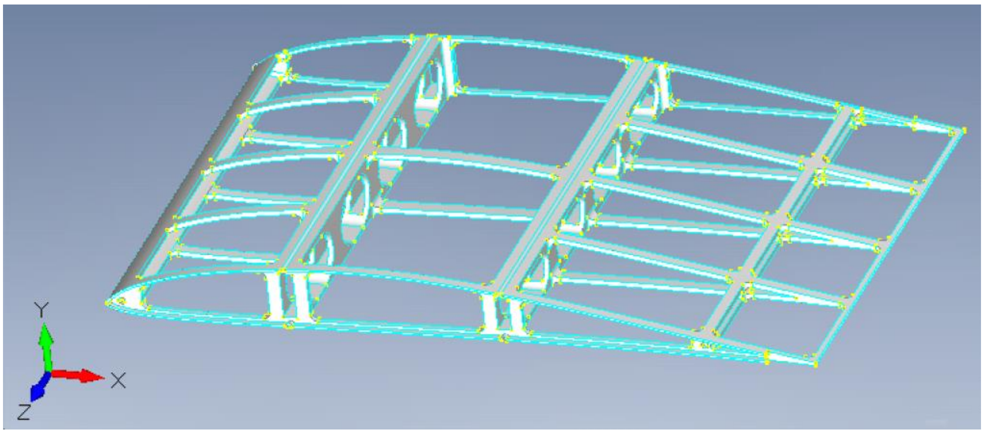

Figure 8: **Parasolid CAD file of a wing section with aileron**

3.2 Detailed finite element model

The Femap code was first used for constructing a detailed model that follows the CAD drawings while representing the actual structural parts by NASTRAN's finite elements. A general view of the detailed model is shown in Fig. 9. It is based on more than 10,000 grid points that yield more than 60,000 DOF. The tip pod is represented by a rigid beam along its center line. Three different material properties are used: Utlem 9085 for the CAD structure, OraCover Light for the wing cover and Aluminum for the two wing spars. The element properties are given in Table 1. The cross sections of the NASTRAN elements that represent the ribs, spars and leading-edge segments are given in Tables 2 to 4.

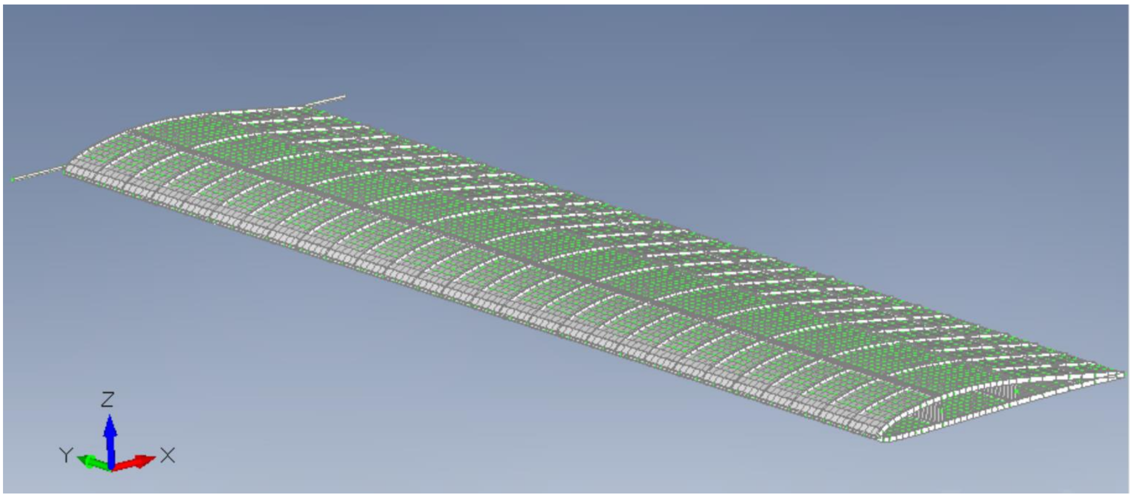

Figure 9: Detailed finite-element model

- *ULTEM 9085*: For the wing body

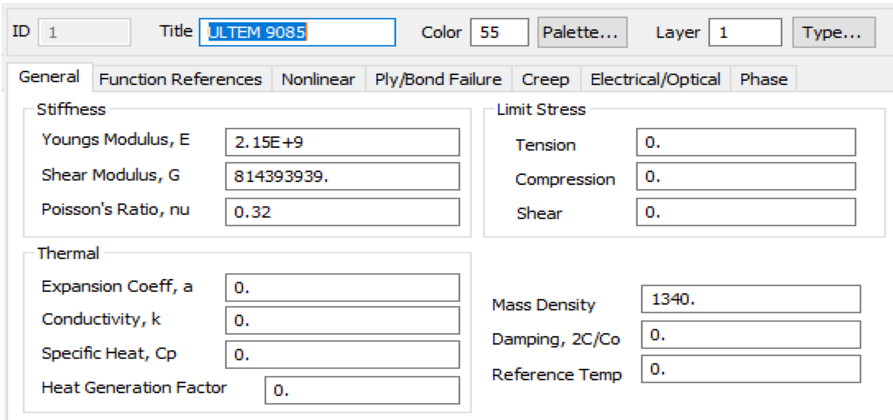

- *OraCover Light*: For the wing skin

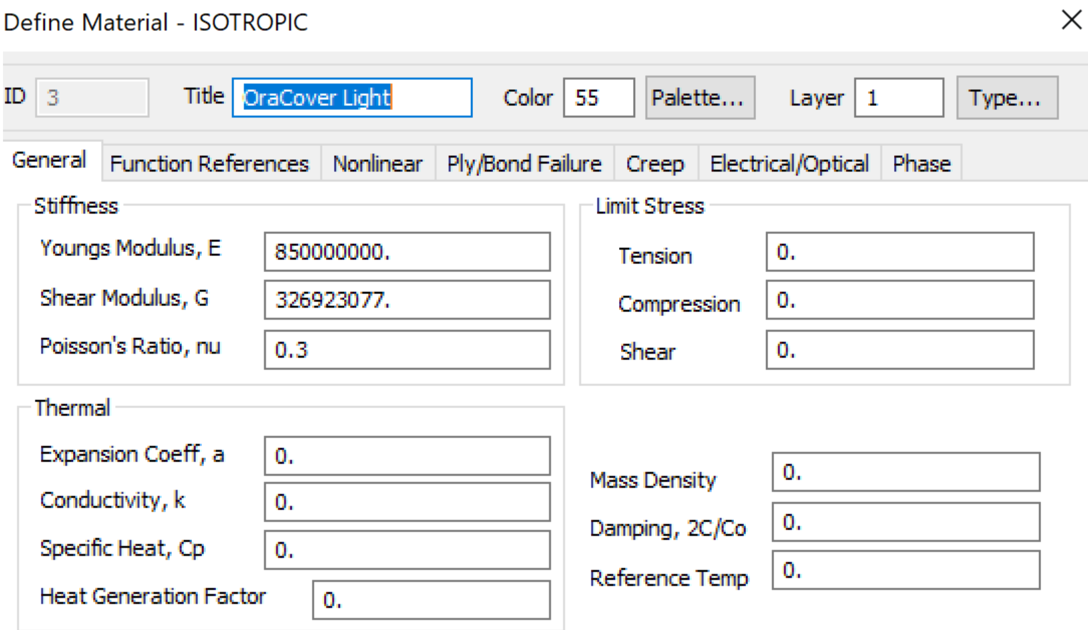

- *Aluminum* : for the wing spars.

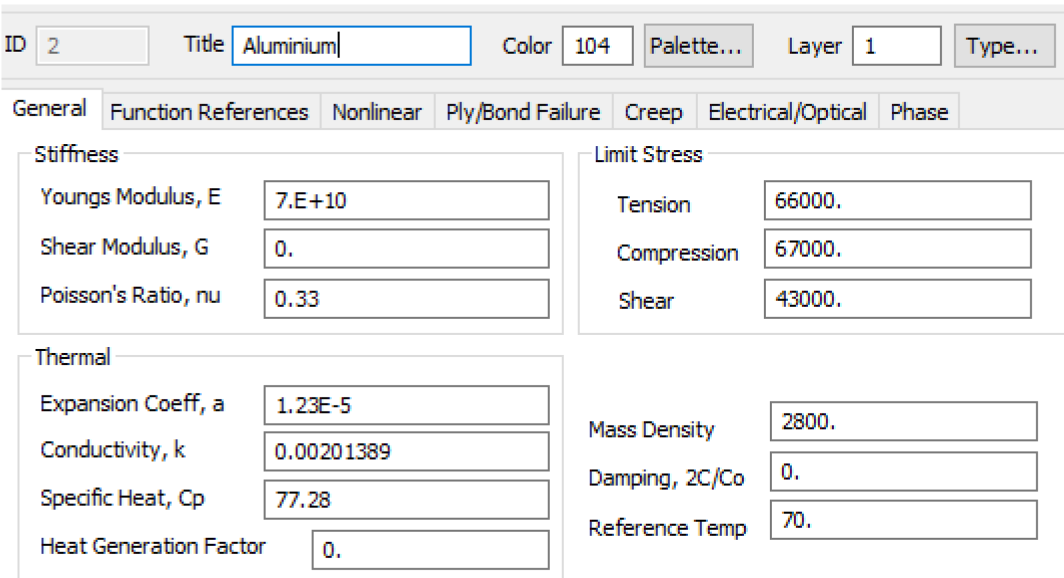

Table 1: Material properties

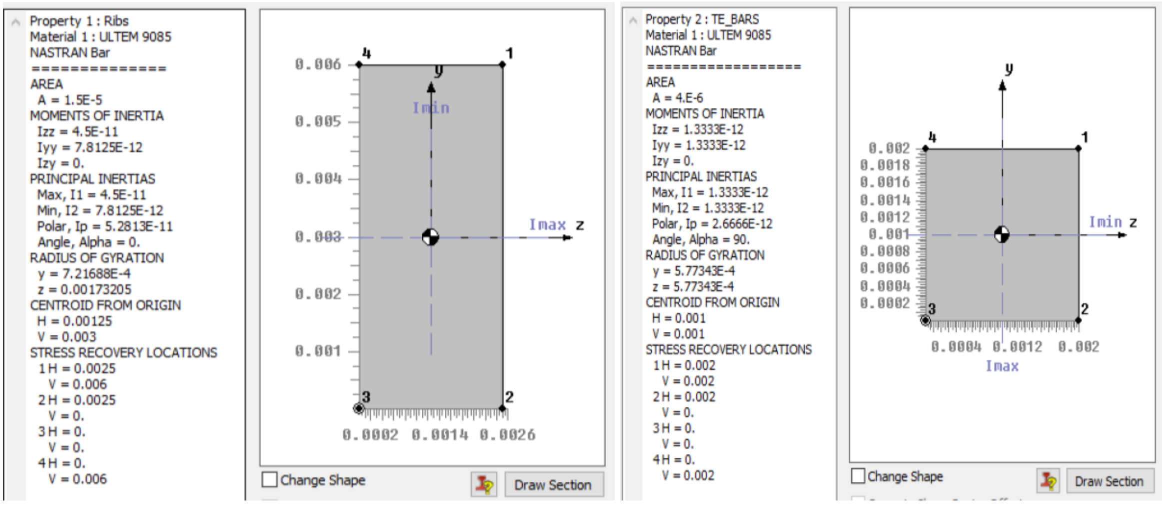

Table 2: Cross sections of forward and rear Ribs represented by BAR elements

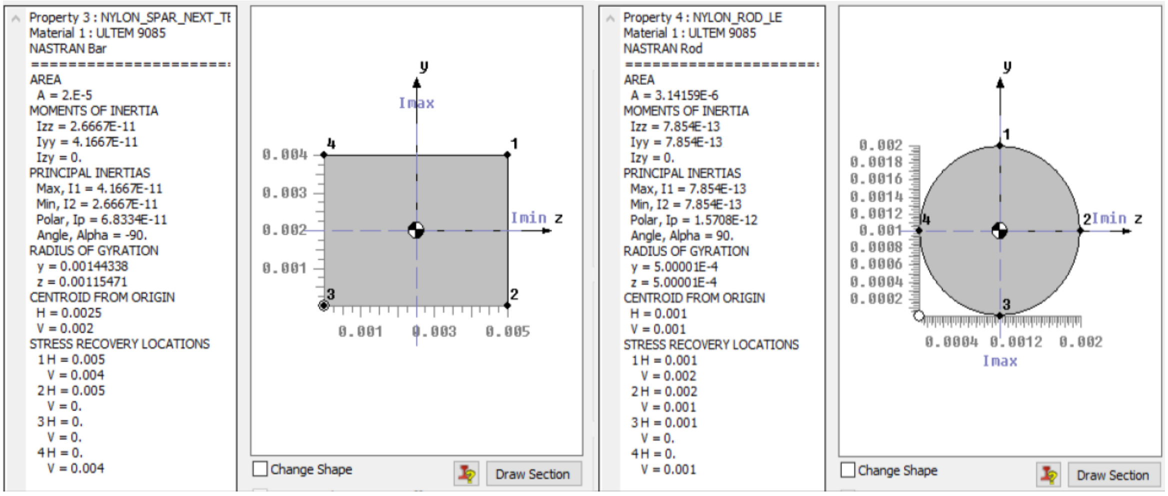

Table 3: Cross sections of ailerod-support BAR elements and leading-edge ROD elements

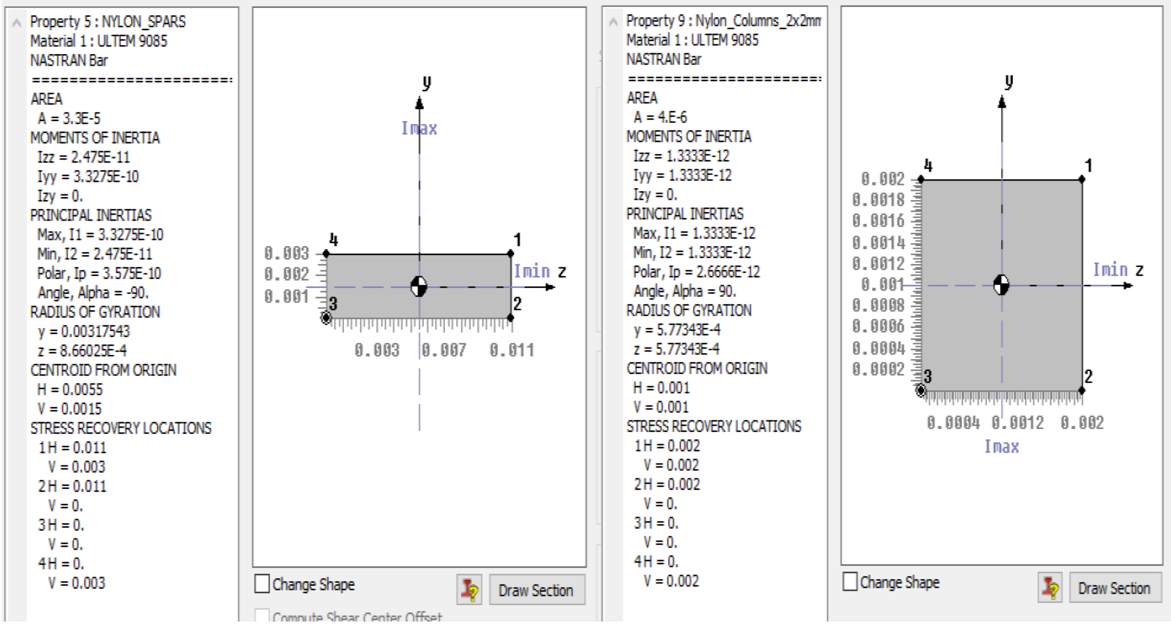

Table 4: Nylon spars and columns around main aluminum spars

3.2 Compact finite element model

The Femap-generated detailed model was used for constructing a compact model of 330 grid points to be used in the preliminary design studies. A general view of the reduced sets of grid points and interconnecting elements is shown in Figure 10. The elements have the cross-section properties shown in Section 3.2 above. The compact model does not have ailerons at this stage. NASTRAN's weight generator, indicating the model total mass properties, is given in Table 5, showing the total weight of 2.35Kg.

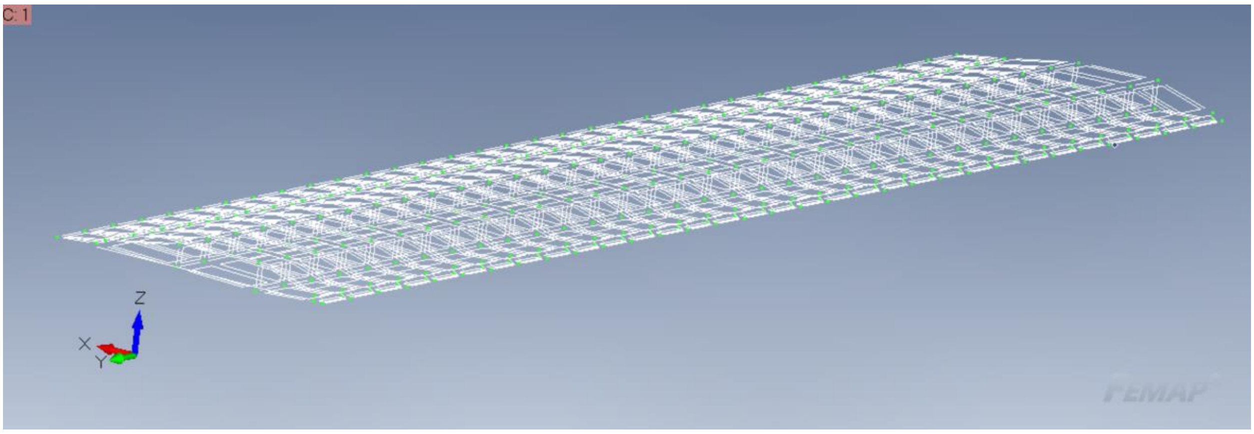

Figure 10: General view of the compact finite-element model

```
          O U T P U T   F R O M   G R I D   P O I N T   W E I G H T   G E N E R A T O R
                                        REFERENCE POINT =        0
                                                  M O
 *  2.346454E+00 -5.181188E-20  2.169887E-18  9.106678E-19  2.108660E-02 -1.479790E+00 *
 * -5.181188E-20  2.346454E+00 -2.006922E-19 -2.108660E-02  7.716677E-21  3.159745E-01 *
 *  2.169887E-18 -2.006922E-19  2.346454E+00  1.479790E+00 -3.159745E-01 -9.183844E-19 *
 *  9.106678E-19 -2.108660E-02  1.479790E+00  1.483680E+00 -1.993659E-01 -2.964607E-03 *
 *  2.108660E-02  7.716677E-21 -3.159745E-01 -1.993659E-01  5.912989E-02 -1.319247E-02 *
 * -1.479790E+00  3.159745E-01 -9.183844E-19 -2.964607E-03 -1.319247E-02  1.541734E+00 *
                                                   S
                     *  1.000000E+00  0.000000E+00  0.000000E+00 *
                     *  0.000000E+00  1.000000E+00  0.000000E+00 *
                     *  0.000000E+00  0.000000E+00  1.000000E+00 *
         DIRECTION
    MASS AXIS SYSTEM (S)     MASS              X-C.G.        Y-C.G.        Z-C.G.
            X            2.346454E+00      3.881038E-19  6.306493E-01  8.986581E-03
            Y            2.346454E+00      1.346604E-01  3.288654E-21  8.986581E-03
            Z            2.346454E+00      1.346604E-01  6.306493E-01 -3.913924E-19
                                                  I(S)
                     *  5.502619E-01  9.681411E-05  1.250766E-04 *
                     *  9.681411E-05  1.639112E-02 -1.057779E-04 *
                     *  1.250766E-04 -1.057779E-04  5.659570E-01 *
                                                  I(Q)
                     *  5.659580E-01                              *
                     *                5.502610E-01                *
                     *                              1.639109E-02 *
                                                   Q
                     *  7.968427E-03 -9.999682E-01  1.812986E-04 *
                     * -1.938728E-04  1.797594E-04  1.000000E+00 *
                     * -9.999682E-01 -7.968461E-03 -1.924342E-04 *
```

Table 5: Mass table of the compact model

3.3 Natural frequencies and normal modes

The results of NASTRAN's normal modes analysis, with the natural frequencies and the generalized mass and stiffness properties, are given in Table 6. The mode shapes associated with the first 6 frequencies are shown in Figure 11.

			R E A L E I G E N V A L U E S			
MODE NO.	EXTRACTION ORDER	EIGENVALUE	RADIANS	CYCLES	GENERALIZED MASS	GENERALIZED STIFFNESS
1	1	1.318092E+03	3.630553E+01	5.778205E+00	1.000000E+00	1.318092E+03
2	2	6.520733E+03	8.075105E+01	1.285193E+01	1.000000E+00	6.520733E+03
3	3	7.406687E+03	8.606211E+01	1.369721E+01	1.000000E+00	7.406687E+03
4	4	4.630175E+04	2.151784E+02	3.424671E+01	1.000000E+00	4.630175E+04
5	5	6.697097E+04	2.587875E+02	4.118731E+01	1.000000E+00	6.697097E+04
6	6	8.052448E+04	2.837684E+02	4.516314E+01	1.000000E+00	8.052448E+04
7	7	2.016622E+05	4.490681E+02	7.147141E+01	1.000000E+00	2.016622E+05
8	8	2.833032E+05	5.322624E+02	8.471219E+01	1.000000E+00	2.833032E+05
9	9	3.334345E+05	5.774379E+02	9.190209E+01	1.000000E+00	3.334345E+05
10	10	3.723001E+05	6.101640E+02	9.711061E+01	1.000000E+00	3.723001E+05

Table 6: Natural frequencies from normal-mode analysis

1. 1^{st} wing bending

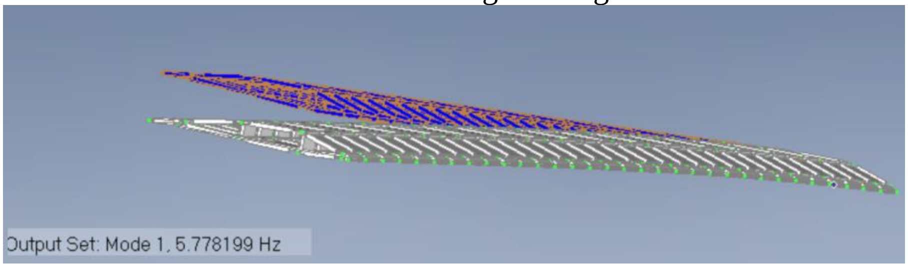

2. 1^{st} wing torsion

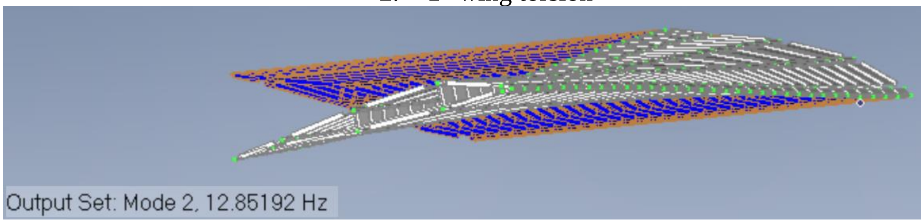

3. Fore & aft wing bending

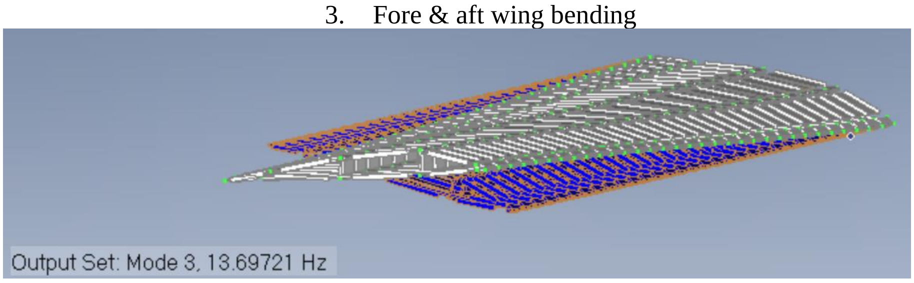

4. 2^{nd} wing bending

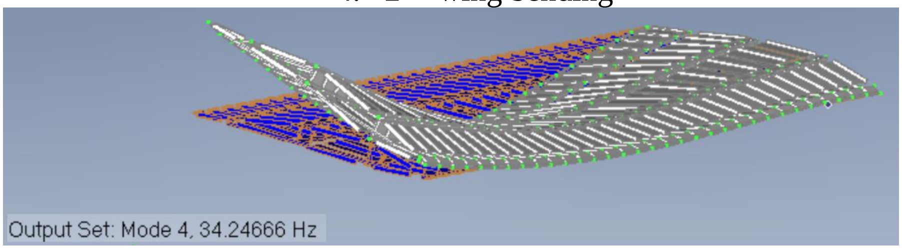

5. 2^{nd} wing torsion

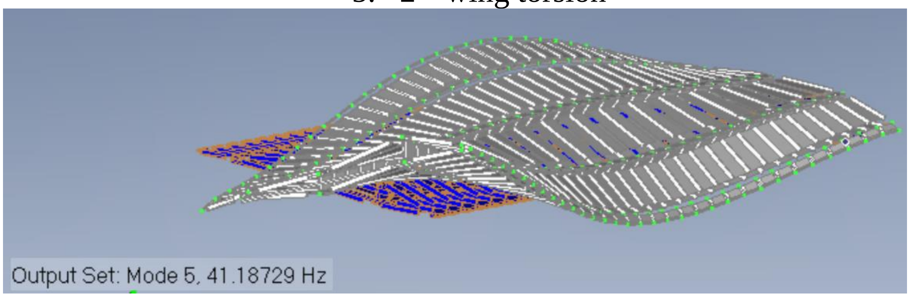

6. 2^{nd} fore & aft wing bending

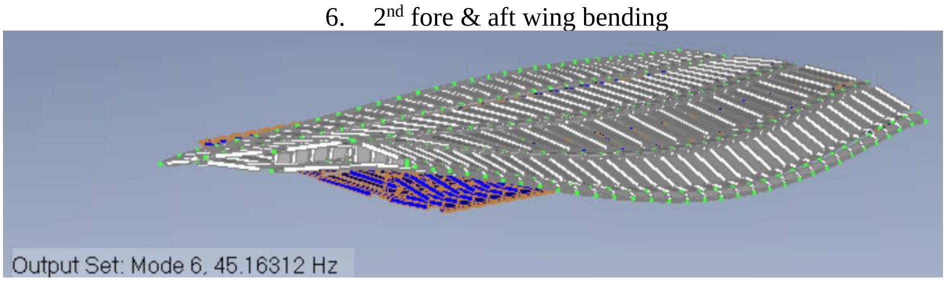

Figure 11: Mode shapes, 1-6, in the structural grid

3.4 **Conventional flutter analysis**

The ZAERO aeroelastic code was used for constructing the panel model for the wing shown in Figure 12. The modal deflections of the previous section are projected to the aerodynamic model using the Infinite-Plate Spline (IPS) technique, based on the upper surface structural displacements. The projected shapes of the first 4 modes are shown in Figure 13, demonstrating that the Spline projection is performed properly.

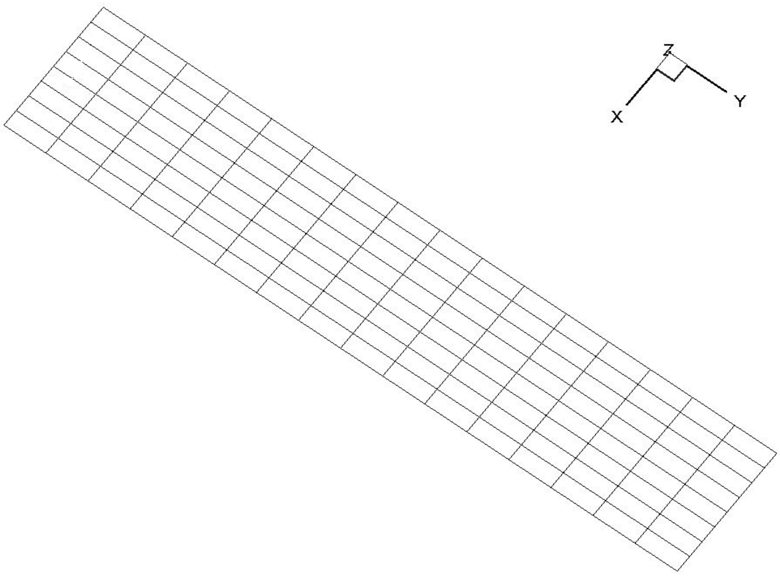

Figure 12: ZAERO aerodynamic model

1st wing bending

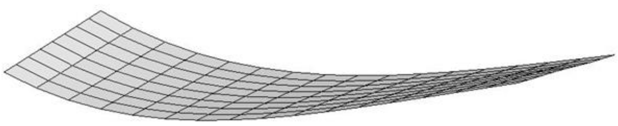

1st wing torsion

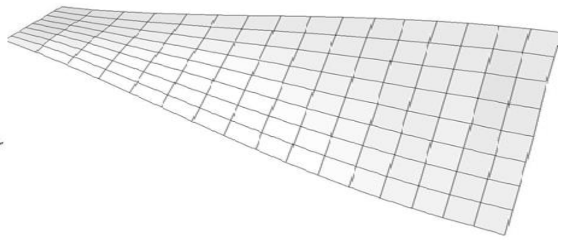

1st fore & aft bending

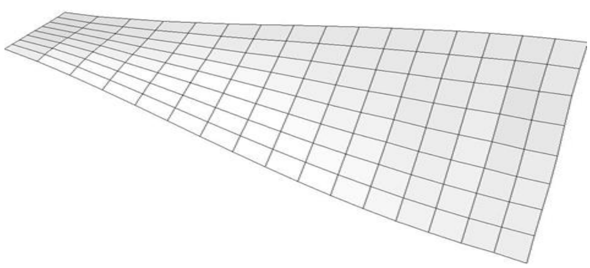

2nd wing bending

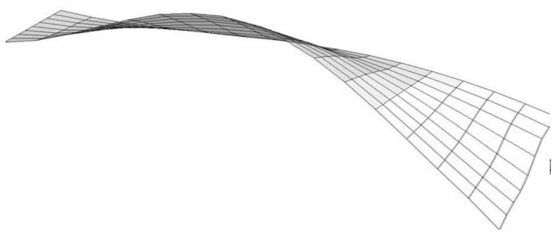

Figure 13: Normal modes in the aerodynamic grid

The conventional flutter analysis was performed using the g method of ZAERO using the first 10 modes of Table 6, with zero structural damping. The significant aeroelastic interaction between the modes in the planned flight envelope is of the first 4 modes, up to 40 Hz. The variations of the aeroelastic frequency and damping coefficients with velocity are shown in Figure 14. The flutter velocity, V_f, is at the first interpolated point where a damping branch crosses the zero line. The flutter frequency, ω_f, is that of the corresponding branch in the frequency plot at V_f. In our case, V_f, = 31.0 m/s and ω_f = 9.2 Hz, as indicated by the red circles in Figure 14. The flutter mode, $\{x_f\}$, is the normalized solution of Eq. (1) with $V=V_f$ and $\omega=\omega_f$.

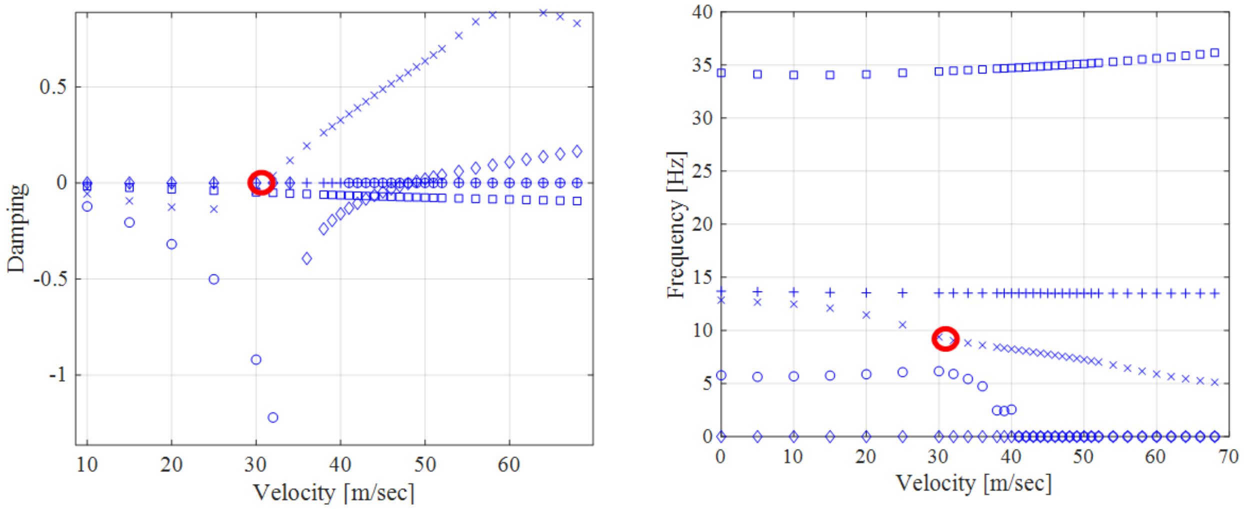

Figure 14: Variations of frequency and damping coefficient vs. velocity, the nominal model

3.5 Flutter margin analysis

The PFM method for flutter analysis is applied using the Dynresp code such that it forms that basis to the planned flutter flight tests. The flutter parameter, P_f, is selected to be a mass term of 0.1Kg in the Z (vertical) direction, located at the tip-section, leading-edge grid point (386). The added mass is applied in Dynresp by a SISO zero-order control system that reads the selected acceleration, y, multiplies it by P_f, and closed the loop by $u=P_f\,y$ to create the system matrix in Eq. (2). These input and output are also kept open for calculating the PFM response of Eq. (2). The Dynresp input file for the PFM analysis that calculated the resulting Bode plots, PFM plots and flutter characteristics, is given in Table 7.

```
SOURCE  ZAERO
AERDATA aerofiles.dat                                   Aero matrices
STRMOD  struct.dat                                      Structural matrices
CSDATA  moti_basic_v5-001.f06                           NASTRAN output
ENDINMAT

TITLE   Assure Flutter
$--1---><--2---><--3---><--4---><--5---><--6---><--7---><--8---><--9---><--10-->
$ FIX = ALT, MARGIN TYPE = FLUTTER
SUBCASE 1
TIMESET 1
STABLE  1
DAMPING 100
AEROSET 10
FCS     1
SMODES  4                                               4 modes only
OUTRES          FORMAT                                                  +
+                       FORMAT

BEGIN BULK
$--1---><--2---><--3---><--4---><--5---><--6---><--7---><--8---><--9---><--10-->
MARGIN  1       FLUTTER 1       ALT     14                              VELS1      Const. alt.
VELS1   10.     15.     20.     25.     27.     29.     31.     33.     VELS2
VELS2   35.     37.     39.     41.     43.     45.                                Velocities
AERO    10      40.     1.225   L       7
MKAEROZ 7       0.85    0.328961                                        REDF1
REDF1   .0      0.01    0.02    0.03    0.04    0.045   0.05    0.055   +
+       0.06    0.062   0.065   0.07    0.075   0.08    0.085   0.09    +          reduced
+       0.1     0.12    0.125   0.13    0.14    0.15    0.2     0.25    +          frequencies
+       0.3     0.4     0.5     0.6     0.7     0.8     0.9     1.0     +
+       1.5
TIMEF1  1       200     0.5     0.05                                           Frequency steps
TABDMP  100                                                             +
+       0.00    0.00    0.99    0.00    1.00    0.00    50.0    0.00         Struct. damping

$ MARGIN "FCS" mass at Grid 368
$--1---><--2---><--3---><--4---><--5---><--6---><--7---><--8---><--9---><--10-->
ASECONT 1               110             300
SENSET  110     11
ASESNSR 11      2       368     3
GAINSET 300     31
ASEGAIN 31      11      1       24      1        .0
CFORCE  24      368     3       1.0

$ Assigning added mass as Flutter parameter
GAINSET 1       310
ASEGAIN 310     11      1       24      1         0.1

ENDDATA
```

Table 7: Dynresp input file for PFM analysis

The Bode plots of gain and phase of the FD acceleration response to unit-amplitude (1N) force applied to the Z direction at the added mass location, vs. frequency, at various velocities, are shown in Figure 15. The phase vs. frequency plots in Fig. 15 are used for extracting the phase-cross-over frequencies for which the flutter gain margins are extracted. The resulting flutter margins (PFM) and phase-cross-over frequencies (WPCO) are plotted vs. velocity in Fig. 16. The PFM=0dB point indicates the flutter velocity, with the added mass removed, and WPCO at this velocity is the flutter frequency. The solution of Eq. (2) with $V=V_f$ and $\omega=\omega_f$ is the flutter mode $\{x_f(i\omega_f)\}$. A comparison between the flutter velocities, frequencies and modes obtained by the ZAERO and Dynresp analyses is given in Table 8, showing practically identical results.

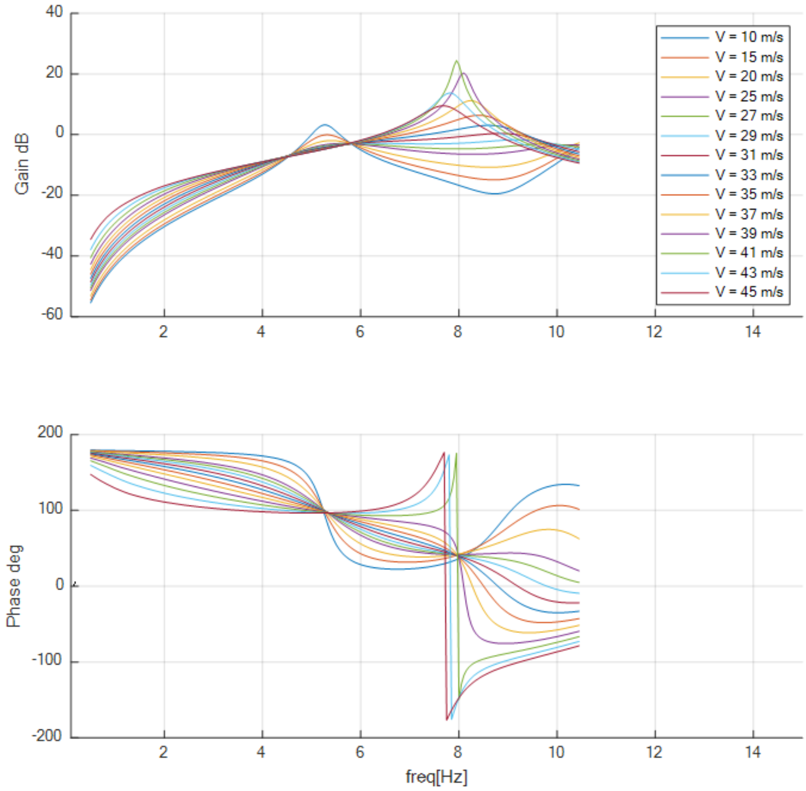

Figure 15: Bode plots of acceleration response to unit-amplitude force at the added mass.

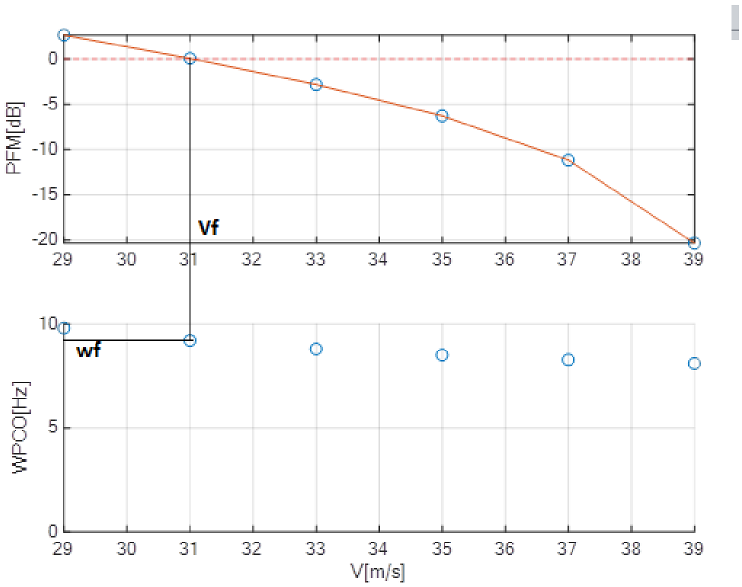

Figure 16: PFM plots: flutter margins and cross-over frequencies vs. velocity.

	ZAERO		DYNRESP	
$V_f\ [\frac{m}{s}]$	31.0342		31.030	
$\omega_f\ [Hz]$	9.2108		9.1927	
ζ_f	1.0	0	1.0	0
	-0.2748	0.2562	-0.27203	0.25295
	-0.1352	0.1166	-0.13392	0.11520
	-0.01409	0.01072	-0.01399	0.01065

Table 8: Flutter characteristics obtained by ZAERO and Dynresp.

4. Active Aeroelastic Aircraft Testbed (A3TB)

4.1 Genral

The A3TB student project model [9] was used in the 2nd year of the project as a test case for the development and application of the methodology for performing safe flutter tests using the PFM approach. A general view of the vehicle and main dimensions are given in Figures 17 and 18. This is a low-cost, experimental, flexible UAV, designed for aeroelastic research and technology demonstration. It is assembled from a fuselage, twelve 3D-printed wing segments and two main spars, one along each wing. General specifications are given in Table 8a. The UAV has eight trailing-edge control surfaces along the wings and it has an electric engine.

Figure 17: General view of the A3TB vehicle

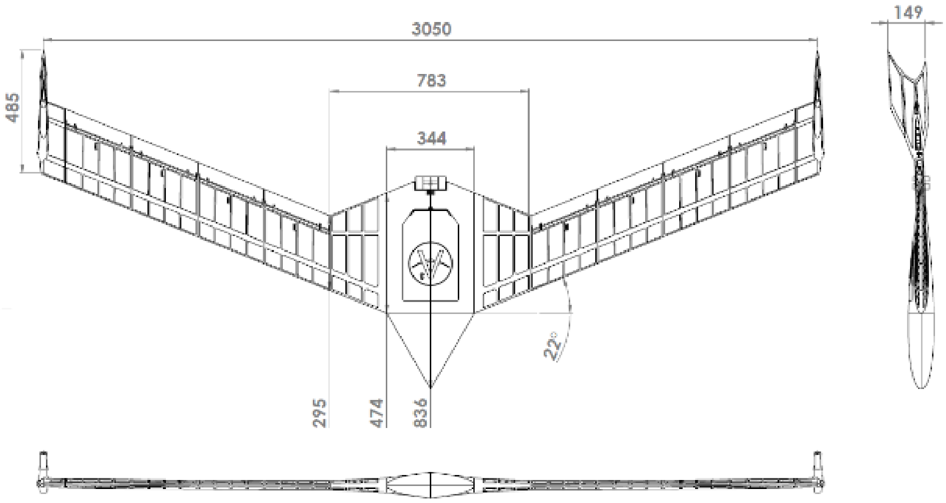

Figure 18: A3TB geometry

Specifications:	Value
Weight	11 Kg.
Sweep angle	22°
Washout torsion angle	3°
Wing span	3048 mm
Aspect Ratio	8.4
Chord length	295 mm

Table 8a: A3TB specifications

4.2 The structural model

A finite-element model was constructed for the right side of the vehicle, with either symmetric or anti-symmetric boundary conditions applied to the grid points in the plane of symmetry. A general view of the MSC/NASTRAN finite-element model of the right side of the vehicle, is shown in Figure 19. The structural model was built in Siemens FEMAP finite-element editing software. The model is built from several types of simple elements such as: beams, bars, plates, and mass. The model materials are ULTEM 9085 plastic, Oracover light, T300 carbon fiber.

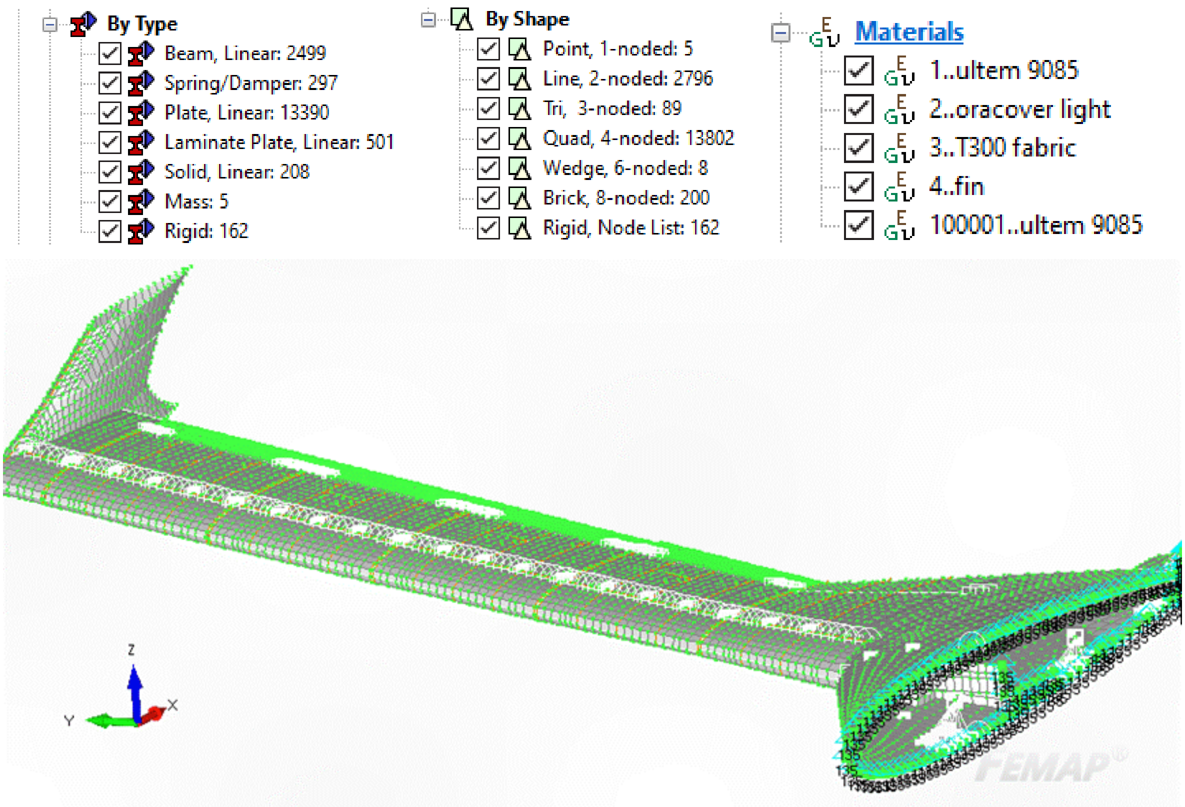

Figure 19: Half-span structural model of A3TB and model properties

4.3 The aerodynamic model

An aerodynamic panel model, shown in Figure 20, was constructed using the ZONA6 module in ZAERO. The model is based on lifting surface panels that represent the wing with its four flaps that serve as both elevators and ailerons, and body panels that represent the fuselage. The aeroelastic analysis requires displacement and force transformations between the structural and aerodynamic models. These transformations are based on Spline techniques: Infinite-Plate Spline for the lifting surfaces and Beam-Spline technique for the fuselage. Modal displacements at structural grid points were exported for this purpose from Nastran's modal analysis to the aeroelastic analysis by the ZAERO code. The grid points used for Spline are marked in Figure .

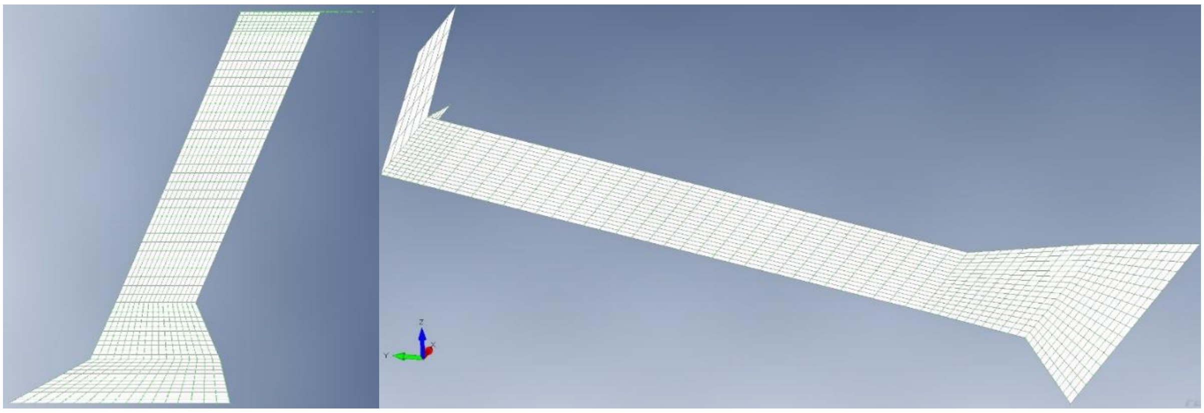

Figure 20: Two views of the aerodynamic model

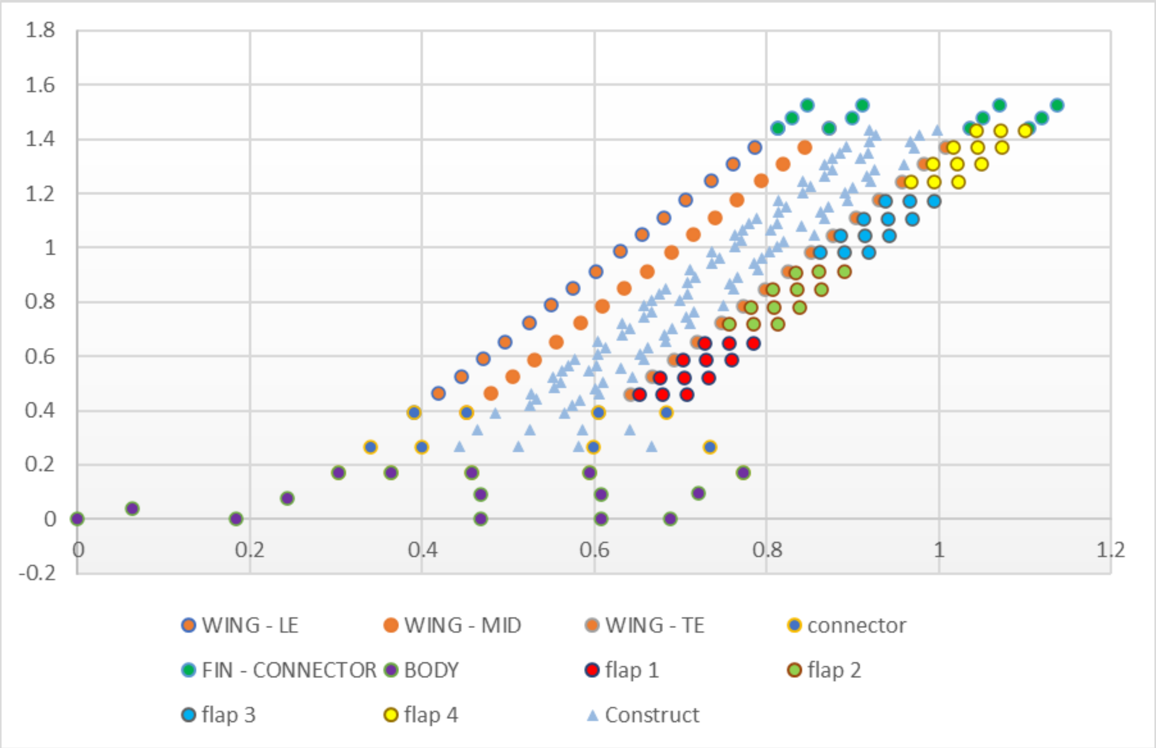

Figure 21: The grid points used for Spline

4.4 Normal modes

Normal modes were calculated for two mass configurations, the nominal one described above, and a modified one with a concentrated mass of 200 gram added at the forward point of the wing-tip section. The second configuration will be used later to validate the PFM sensitivity analysis. The resulting fundamental frequencies and mode descriptions are given in Table 9. The respective symmetric and anti-symmetric mode shapes of the nominal configuration are shown in the aerodynamic grid in Figures 21 and 22. It may be noticed that the 1st symmetric mode reflects reflect (a) significant coupling between bending and torsion due to the rear CG of the outboard sections compared to the main spar; and (b) the small pitch moment of inertia of the fuselage compared to conventional air vehicles. These couplings have significant effects of the flutter mechanisms described in Section 4.5.

Mode Number	Symmetric Nominal $[Hz]$	Symmetric +200gr $[Hz]$	Description	Anti-symmetric Nominal $[Hz]$	Anti-symmetric +200gr $[Hz]$	Description
1	0.00	0.00	Rigid body	0.00	0.00	Rigid body
2	0.00	0.00	Rigid body	0.00	0.00	Rigid body
3	0.00	0.00	Rigid body	0.00	0.00	Rigid body
4	6.80	6.67	1st bending	9.16	7.92	1st torsion
5	9.85	8.55	F&A bending	17.76	17.16	1st bending
6	11.32	9.20	1st torsion	21.86	21.10	F&A bending
7	19.12	19.11	2nd bending	26.24	25.68	2nd bending
8	29.83	28.71	2nd torsion	28.95	25.97	2nd torsion

Table 9: A3TB fundamental natural frequencies

6.80 Hz., 1^{st} bending

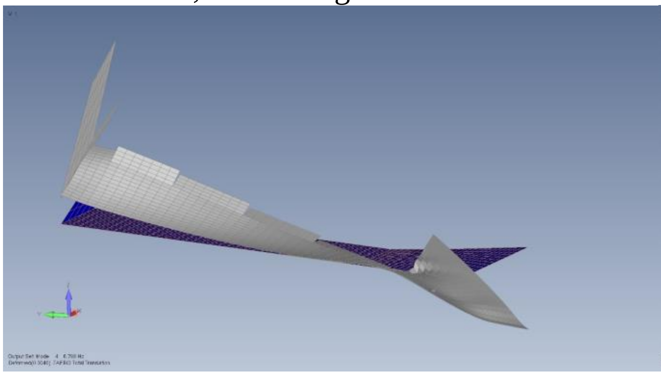

9.85 Hz., F&A bending

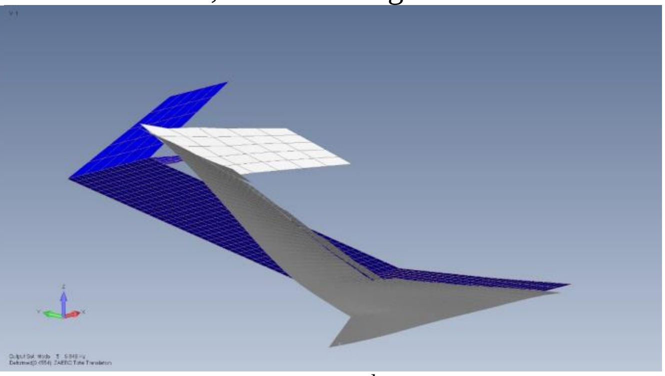

11.32 Hz. 1^{st} torsion

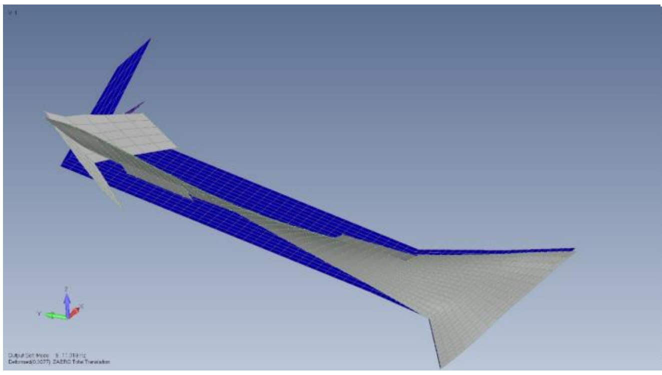

19.12 Hz., 2^{nd} bending

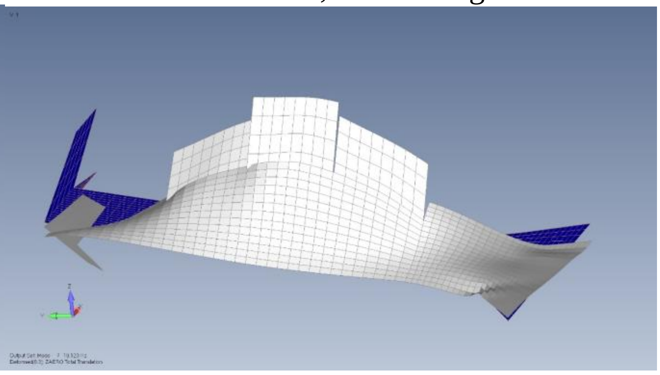

Figure 21 Symmetric normal modes 4-8

19.16 Hz., 1^{st} torsion

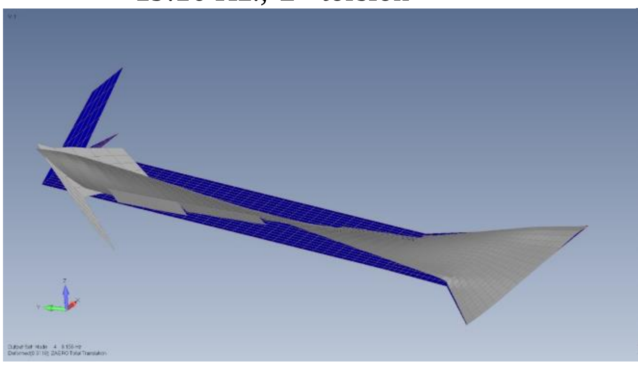

17.76 Hz., 1^{st} bending

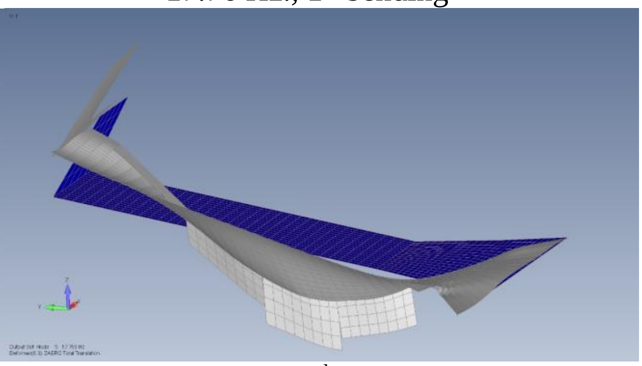

21.86 Hz., F&A bending

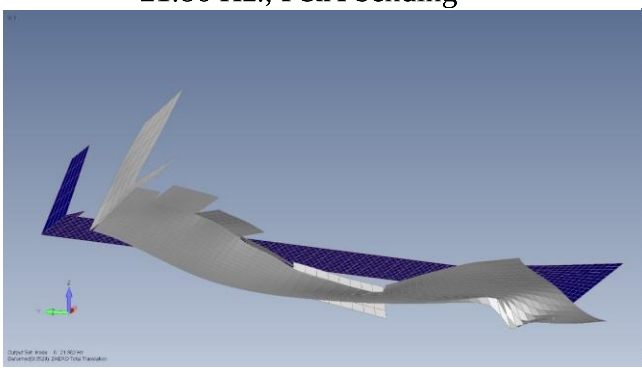

26.24 Hz., 2^{nd} bending

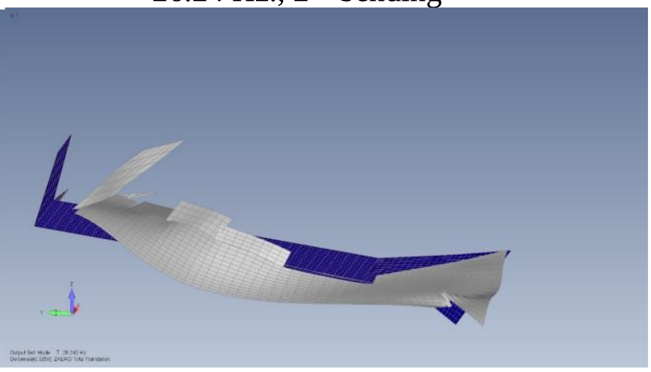

Figure 22: Anti-symmetric normal modes 4-8

4.5 Flutter analysis using ZAERO

Open-loop flutter analyses was performed using the g-method option of the ZAERO software package, assuming 2% structural damping with the 8 modes of Table 8 considered in each case. The symmetric and anti-symmetric V-g plots of the nominal configuration are given in Figures 23 and 24 respectively. The respective V-g plots of the “+200gr” configuration are shown in Figures 25 and 26. The resulting flutter characteristics are summarized in Table 9a.

Configuration	Boundary conditions	Flutter velocity (m/s)	Flutter frequency (Hz.)	Flutter mechanism	Figure
Nominal	Sym	24.48	8.49	Wing torsion-bending	23
	Anti	26.27	6.36	Wing torsion-roll	24
+200 gr	Sym	25.90	7.21	Wing torsion-bending	25
	Anti	32.10	5.56	Wing torsion-roll	26

Table 9a: A3TB Flutter characteristics

It can be observed that the lowest flutter velocity in both configurations is symmetric. While the symmetric flutter mechanism is of a classic torsion-bending interaction, the anti-symmetric one is of the interaction of wing torsion and rigid-body roll, a mechanism that is often called “body-freedom flutter”. In both mechanisms, the added mass increases the flutter velocity, as forward-located masses often do.

It may also be noticed that the critical torsion-bending mechanism in Figure 23 turns in Figure 25 into a more moderate “hump-mode” flutter, namely with the damping branch crossing the zero line back to the stable zone. However, the flutter velocity increase is only 6% even though the 200-gram mass increase is quite significant with respect to the ~5Kg half-aircraft weight. A more thorough sensitivity study is conducted in the next section.

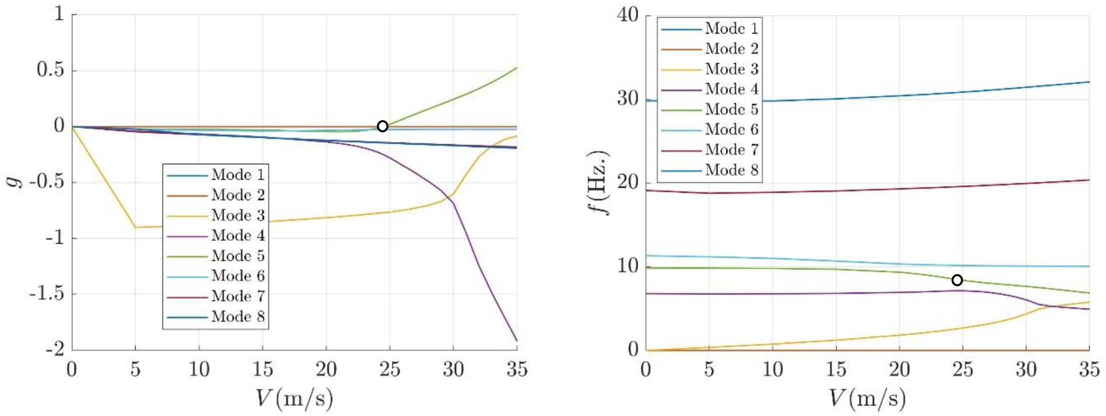

Figure 23: A3TB nominal symmetric flutter results

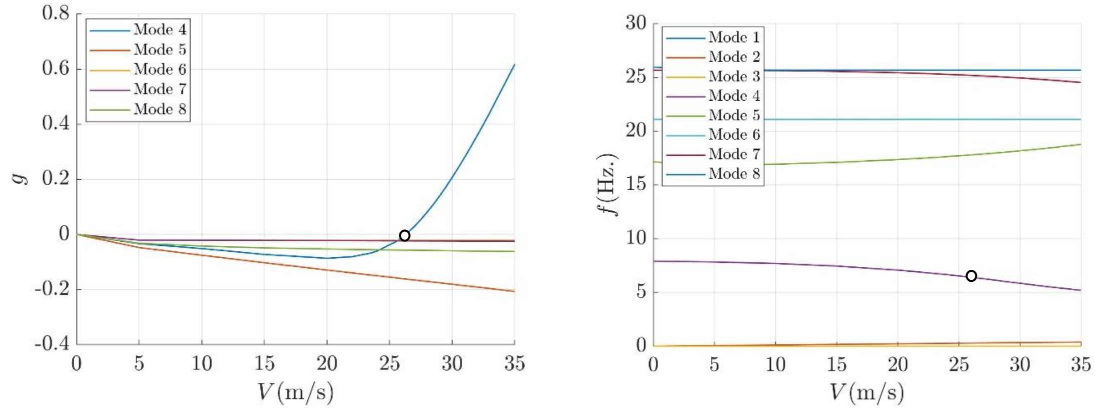

Figure 24: A3TB nominal anti-symmetric flutter results

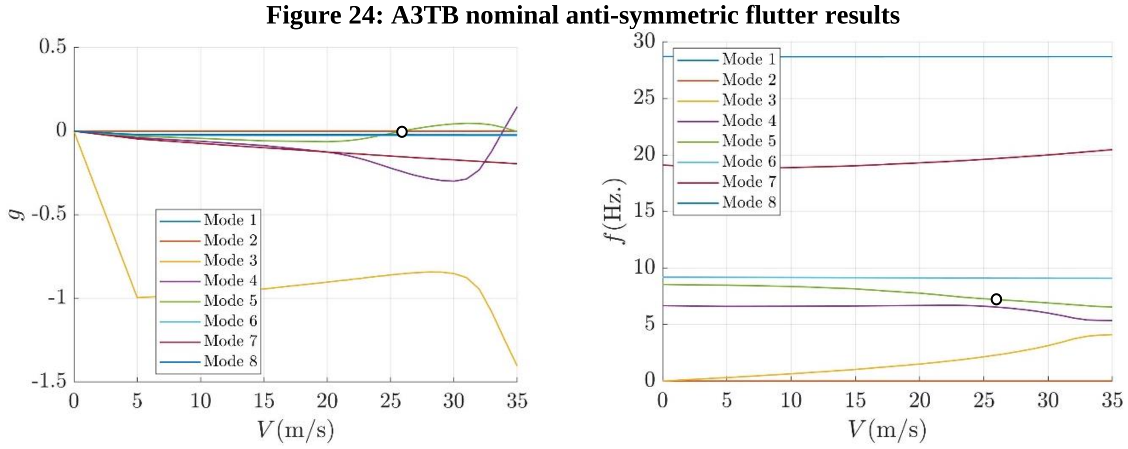

Figure 25: A3TB with 200-gram wingtip mass symmetric flutter results

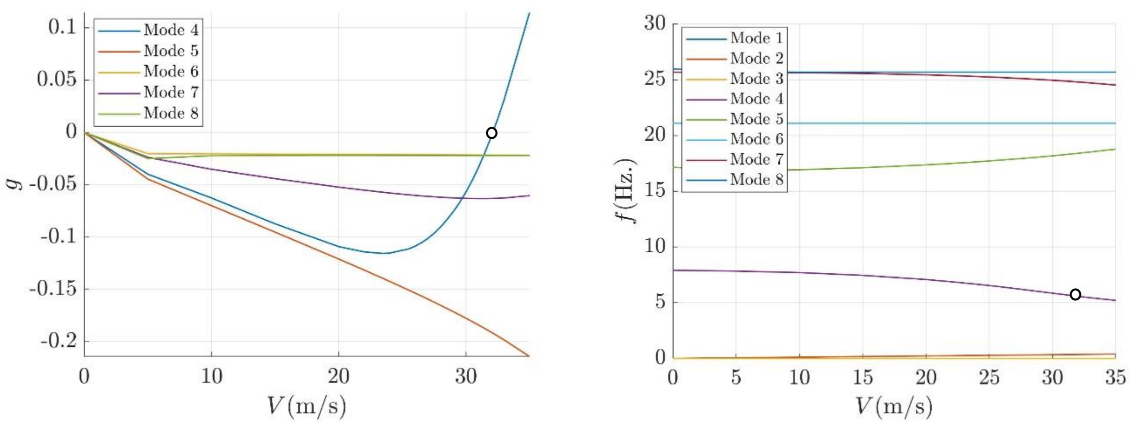

Figure 26: A3TB with 200-gram added mass anti-symmetric flutter results

4.6 Flutter sensitivity to varying mass using Dynresp

Flutter sensitivity analysis was performed, using the Dynresp code, to identify the best size and location for the added mass in PFM flutter tests. As a first step, the +200gr dynamic model of Section 4.4, with the added 200 grams at the forward point of the wing-tip section (GRID 29880), served as a baseline model. This point is marked at No. 1 in the structural grid plot in Figure 27.

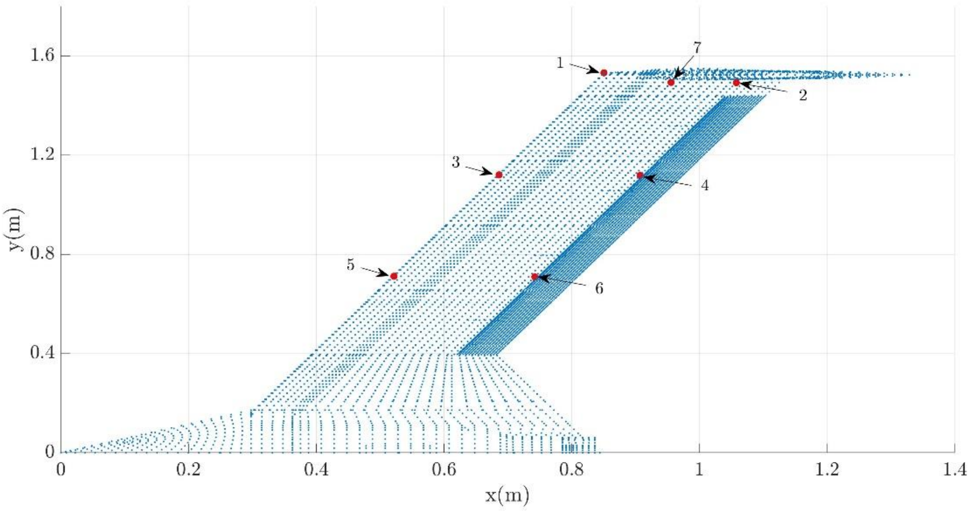

Figure 27: Structural grid points with added mass locations

To prepare the symmetric modal and the unsteady aerodynamic data needed for the Dynresp run, the symmetric 200gr ZAERO run was repeated with OUTPUT4 cards of Table 10 added to export the generalized mass, stiffness and aero matrices, MHH, KHH and the 31 QHH(*ik*) matrices, to the MTR folder.

```
$--1---><--2---><--3---><--4---><--5---><--6---><--7---><--8---><--9---><--10-->
OUTPUT4 QHHS0101MTR/QHHS0101.DAT
OUTPUT4 QHHS0102MTR/QHHS0102.DAT
OUTPUT4 QHHS0103MTR/QHHS0103.DAT
OUTPUT4 QHHS0104MTR/QHHS0104.DAT
OUTPUT4 QHHS0105MTR/QHHS0105.DAT
OUTPUT4 QHHS0106MTR/QHHS0106.DAT
OUTPUT4 QHHS0107MTR/QHHS0107.DAT
OUTPUT4 QHHS0108MTR/QHHS0108.DAT
OUTPUT4 QHHS0109MTR/QHHS0109.DAT
OUTPUT4 QHHS0110MTR/QHHS0110.DAT
OUTPUT4 QHHS0111MTR/QHHS0111.DAT
OUTPUT4 QHHS0112MTR/QHHS0112.DAT
OUTPUT4 QHHS0113MTR/QHHS0113.DAT
OUTPUT4 QHHS0114MTR/QHHS0114.DAT
OUTPUT4 QHHS0115MTR/QHHS0115.DAT
OUTPUT4 QHHS0116MTR/QHHS0116.DAT
OUTPUT4 QHHS0117MTR/QHHS0117.DAT
OUTPUT4 QHHS0118MTR/QHHS0118.DAT
OUTPUT4 QHHS0119MTR/QHHS0119.DAT
OUTPUT4 QHHS0120MTR/QHHS0120.DAT
OUTPUT4 QHHS0121MTR/QHHS0121.DAT
OUTPUT4 QHHS0122MTR/QHHS0122.DAT
OUTPUT4 QHHS0123MTR/QHHS0123.DAT
OUTPUT4 QHHS0124MTR/QHHS0124.DAT
OUTPUT4 QHHS0125MTR/QHHS0125.DAT
OUTPUT4 QHHS0126MTR/QHHS0126.DAT
OUTPUT4 QHHS0127MTR/QHHS0127.DAT
OUTPUT4 QHHS0128MTR/QHHS0128.DAT
OUTPUT4 QHHS0129MTR/QHHS0129.DAT
```

```
OUTPUT4 QHHS0130MTR/QHHS0130.DAT
OUTPUT4 QHHS0131MTR/QHHS0131.DAT

OUTPUT4 SMHH    MTR/SMHH.DAT
OUTPUT4 SKHH    MTR/SKHH.DAT
```

Table 10: Generalized aero and structural matrices for Dynresp flutter analysis.

The list of Table 10 was also written in the respective `aerocards.dat` and `struct.dat` files for use by Dynresp. The `A3TB_V4_chopped_fin_sym_200gm.f06` NASTRAN file with the modal displacements of the structural sensor points was also generated for use by Dynresp. The Dynresp .inp file for flutter analysis is given in Table 11. The ZAERO- and NASTRAN-generated data served as inputs to the Dinresp flutter run. The ASEGAIN 31 card implies that the flutter parameter P_f is in our case and additional mass of 0.2Kg at Point 1, with which Eq. (7) is solved for the frequency response function (FRF), $y_f(i\omega)$, of the local acceleration to the applied local unit force, $u_f(i\omega)$=(1.,0.), both in the Z direction.

```
SOURCE  ZAERO
AERDATA aerocards.dat
STRMOD  struct.dat                                  } Input data files
CSDATA  A3TB_V4_chopped_fin_sym_200gm.f06
ENDINMAT
TITLE   A3TB Pf=200gr at wing tip fwd
$--1---><--2---><--3---><--4---><--5---><--6---><--7---><--8---><--9---><--10-->
SUBCASE 1
TIMESET 1                                     refers to TIMEF1 card
STABLE  1                                     refers to MARGIN card
DAMPING 20                                    refers to TABDMP card
AEROSET 1                                     refers to AERO card
FCS     1                                     refers to ASECONT card
OUTRES                                                                  +
+                       FORMAT                requests .f118 output file

BEGIN BULK

MARGIN  1       FLUTTER 100     ALT     23                              +FIX0
+FIX0   5.0     10.0    15.0    20.0    21.0    21.5    22.0    22.5    +FIX1
+FIX1   23.0    23.5    24.2    24.5    25.0    25.5    26.0    27.5    +FIX2
+FIX2   29.0    30.0    31.0    32.0    33.0    34.0    35.0

$--1---><--2---><--3---><--4---><--5---><--6---><--7---><--8---><--9---><--10-->
AERO    1       30.     1.225   L       1000
MKAEROZ 1000    0.15    0.3                                             +MK1
+MK1    0.005   0.01    0.02    0.03    0.04    0.05    0.06    0.08    +MK2
+MK2    0.1     0.11    0.12    0.13    0.14    0.15    0.16    0.17    +MK3
+MK3    0.18    0.2     0.3     0.4     0.5     0.6     0.7     0.8     +MK4
+MK4    1.0     1.5     2.0     2.5     3.0     5.0

TIMEF1  1       200     3.0     0.05
$--1---><--2---><--3---><--4---><--5---><--6---><--7---><--8---><--9---><--10-->
$ “control system” that defines acceleration sensor, gain (added mass) and
$ feedback force.
ASECONT 1               180             910
SENSET  180     101
ASESNSR 101     2       29880   3
GAINSET 910     30
ASEGAIN 30      101     1       300     1       0.0
$ selected gain that defines the Pf parameter (additional 200grams).  This gain
$ is not included in the control feedback.
GAINSET 100     31                                        referred by MARGIN card
ASEGAIN 31      101     1       300     1       0.2       referred by GAINSET 100 card
CFORCE  300     29880   3       1.0                       referred by ASEGAIN cards
ENDDATA
```

Table 11: Dynresp input file for flutter analysis.

The FRFs $y_f(V;i\omega)$ were calculated in Dynresp for selected air velocities between 24 and 35m/s. Cross-over frequencies, ω_{co}, at which $\Phi = \angle\left(y_f(i\omega)\right) = \pm 360^o n$, and the corresponding gains $y_f(\omega_{co})$, which are positive real numbers, were used for calculating ΔP_f of Eq. (11), were calculated for each velocity. In our case, ΔP_f is the mass increment Δm needed to cause the current velocity to become a flutter-boundary point V_f. Every velocity may yield several cross-over frequencies that correspond to different Δm values associated with different flutter mechanisms.

The variations of $\Delta m = \Delta P_f$ and $f = \omega_{co}$ with air velocity, corresponding to all the velocity point at which one or more phase-cross-over frequency points exist, are shown in Figures 28 and 29 for symmetric and antisymmetric flutter respectively. Since the baseline NASTRAN model in this case is with +200gr, the corresponding flutter velocities are those at which a Δm branch crosses the zero line. These velocities, and the corresponding flutter frequencies are compared to the ZAERO results in the "+200 gr" lines of Table 12, demonstrating practically identical results.

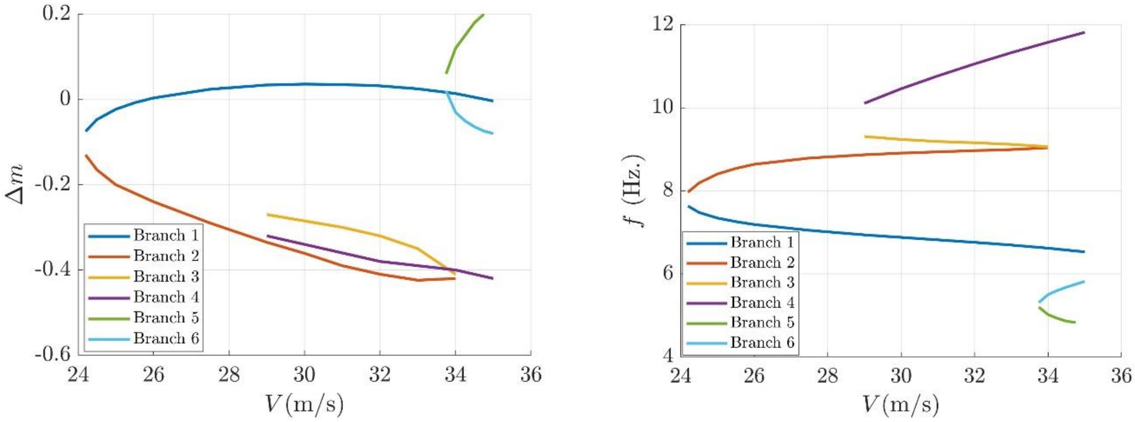

Figure 28: A3TB Dynresp symmetric flutter V-Delta and V-f plots, starting with +200gr.

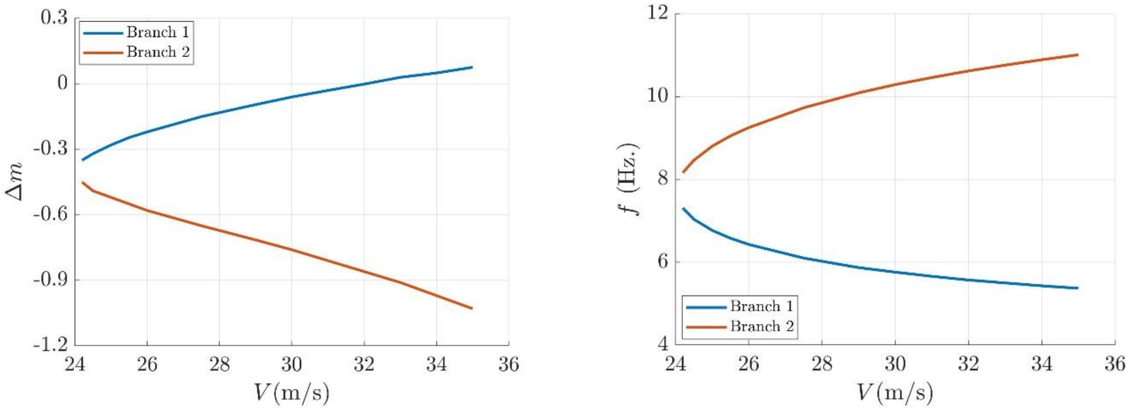

Figure 29: A3TB Dynresp anti-symmetric flutter V-Delta and V-f plots, starting with +200gr.

		ZAERO		Dynresp (SISO)	
Case	Symmetry	Flutter velocity (m/s)	Flutter frequency (Hz.)	Flutter velocity (m/s)	Flutter frequency (Hz.)
Nominal	Sym	24.48	8.49	25.02 (24.46)	8.41(8.49)
+200 gr		25.90	7.21	25.84	7.21
Nominal	A-Sym	26.27	6.36	26.22 (26.25)	6.37 (6.38)
+200 gr		32.10	5.56	32.03	5.57

Table12: Flutter velocities and frequencies in ZAERO and Dynresp

The plots in Figures 28 and 29 also reveal the flutter sensitivity to variations in Δm, this time starting from the "+200 gr" configuration. The flutter velocities and frequencies expected, for example, for the nominal structure are those at which a Δm branch crosses the -0.2 line. The resulting symmetric flutter characteristics are V_f =25.02 m/s, ω_f =8.41 Hz. As shown in the "Nominal" lines of Table 12, these results are not as accurate as the +200gr ones, but we need to realize that: (a) the two sets of nominal results are calculated with different modes; and (b) the used SISO-PFM method allows the removal of mass in one direction only (obviously, we removed the mass in the Z direction).

Rerun of Dynresp with the nominal modes imported from NASTRAN (without the 200 gr) and with $P_f = 0.4$Kg resulted in practically identical results to ZAERO. The Δm and frequency plots are given in Figures 30 and 31. The results are similar to those of Figures 28 and 29, shifted 0.2Kg up due to the wingtip mass difference between the two configurations. The flutter results are given in parenthesis in the "Nominal" lines of Table 12. Despite the slight difference of the symmetric results, sensitivity analyses performed in a single run, with one set of NASTRAN modes, are considered adequately accurate for design purposes. Figure 30 reveals, for example, that an addition of more than 250 grams at Point 1 increases the flutter velocity from 24 to more than 33m/s with the flutter frequency reduced to about 5Hz. With less than 80 grams the flutter velocity is reduced, and with 80 to 250 grams the flutter velocity is increased up to 29m/s.

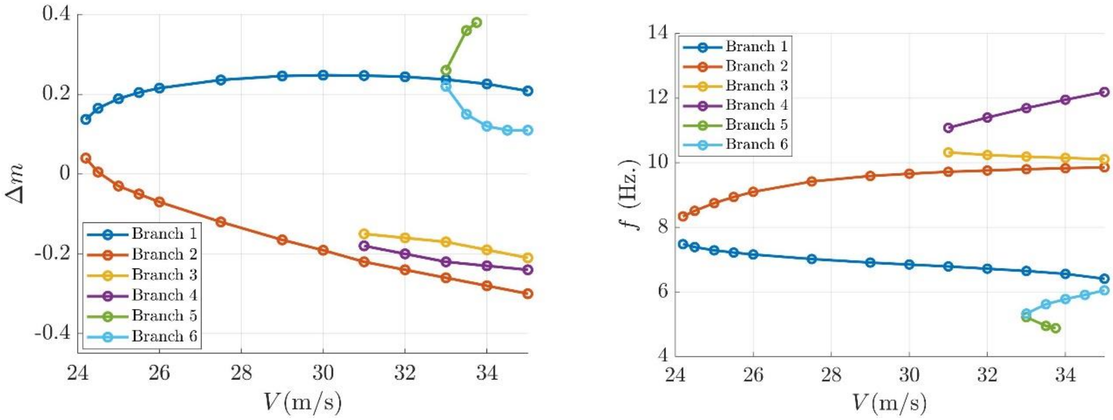

Figure 30: Case1 symmetric flutter V-Delta and V-f plots

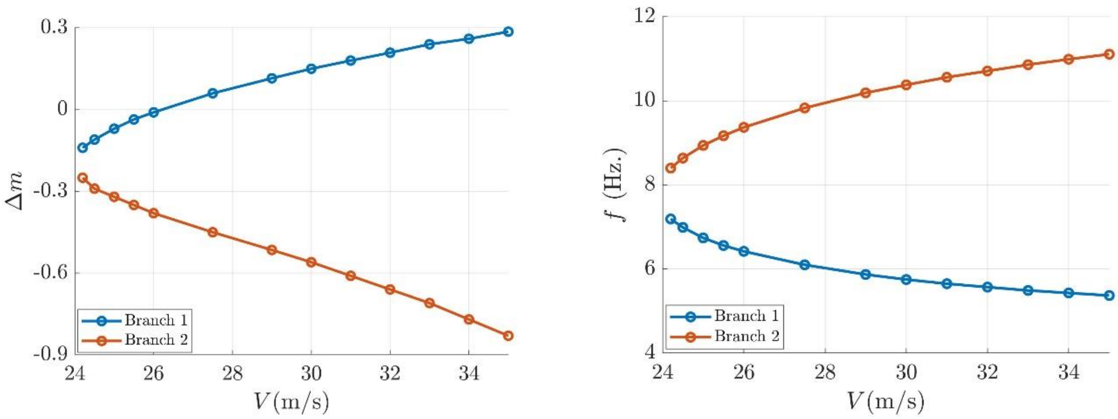

Figure 31: Case1 anti-symmetric flutter V-Delta and V-f plots

4.6 Optimal shaker location

The optimal shaker location for safe flutter tests depends on its effectivity (per mass) in increasing the flutter velocity and in the resulting local vibration level. There are of course other practical considerations such as geometric limitations, accessibility and shaker availability that we ignore at this stage.

To demonstrate a search for optimal location, we repeated the sensitivity analysis of Figures 30 and 31 for six other locations marked as 2 to 7 in Figure 27, naming the sensitivity cases as Case 1 to Case 7. The resulting symmetric and antisymmetric Δm vs. V plots are first converted, for convenience into V_f vs. Δm plots, considering the positive mass increments only. The resulting flutter sensitivity plots for Cases 1 and 2 are given in Figure 32.

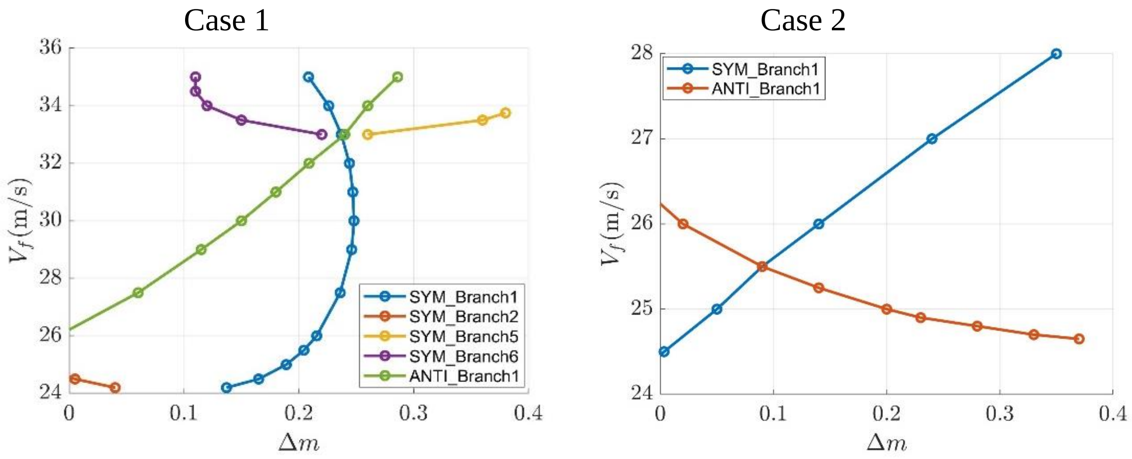

Figure 32: Flutter velocity vs. added mass, Cases 1 and 2

The results of interest in Figure 32, for highest mass effectivity, are of the smallest flutter velocity at each *Δm*. The assembly of these points in Cases 1 through 7 is shown in Figure 33. It can be deduced that the most effective added mass locations, for obtaining highest minimal flutter velocity, are Points 1 and 7. Point 7 (middle of the tip-section chord) is most effective for total shaker weight of up to 0.22 Kg, and Point 1 (leading edge of tip section) is most effective with a higher shaker wight. The mass at Point 7 reduces the flutter velocity by simply reducing the bending frequency without changing the torsion one. The mass at Point 1 reduces both frequencies, but also changes the bending-torsion coupling in a manner that is very effective with high added mass values.

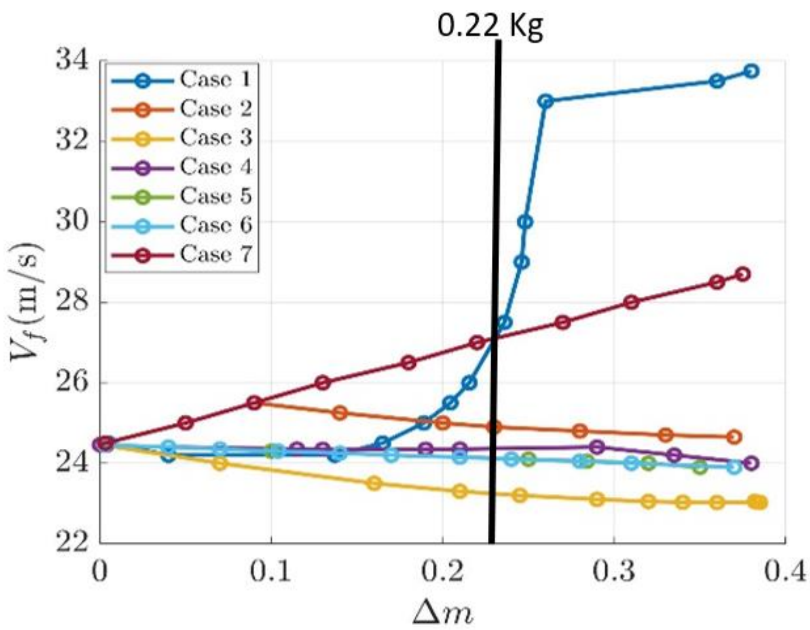

Figure 33: Lowest flutter velocity vs. added mass, Cases 1 through 7

4.7 Validation of case 1 results with output responses (.f58)

The FD output response $y(i\omega)$ to an unit input is provided in the .f58 output file for each subcase of the STABLE analysis type. The output is measured here at the accelerometer attached to point 29880 and the input is a 1N sinusoidal excitation to the mass of 0.4 Kg located at the same point 29880. Since the output is for unit input, the gain and phase of the frequency response can be obtained as,

$$G = |y(i\omega)|,\ \ \phi = arg\big(y(i\omega)\big) \tag{12}$$

The phase-cross-over frequency is the frequency at which phase becomes zero. Thus, $\arg\left(y_f(\omega_{co})\right)=0$. The corresponding real-valued frequency response, $y_f(\omega_{co})$, can be used to obtain the incremental $\Delta m = \Delta P_f$ to obtain flutter at the current velocity point. Here, we are repeating our earlier analysis in section 4.5. So, we expect to get the same results. The comparison of the and cross-over frequencies at various velocities in the symmetric case are shown in Figures 34. The results match exactly those of Figure 30, but now we have some extra points, with Δm>0.4, that were not obtained in Figure 30. These points correspond to $y_f(\omega_{co})<0$ range that is not considered in the flutter boundary search of Dynresp. It may be noticed that there is some irregularity in the Δm plot, when Δm crosses the 0.4 line, because the system matrix in Eq. (7) is singular at this point. Still, the results indicate that good results may be obtained near this singularity. These comparisons serve as a validation of the Matlab analysis tool used in the flutter margin calculations of the following section.

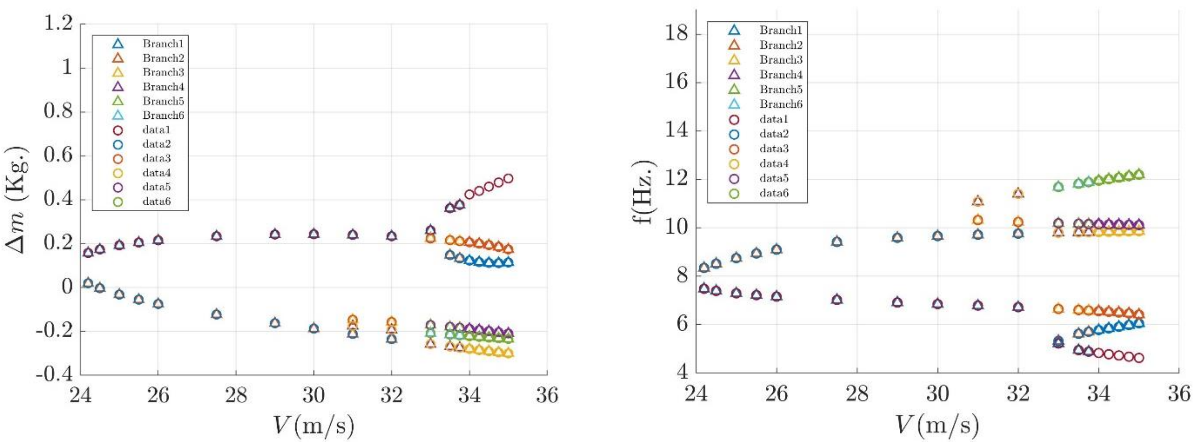

Figure 34: Case 1 symmetric, comparison of Δm and phase-cross-over frequencies

4.8 Flutter margins with atmospheric turbulence noise

Here, we intend to perform a stability analysis in presence of atmospheric turbulence by analyzing the accelerometer responses of the wing with a shaker of fixed mass attached to it. This analysis is expected to provide results analogous to a flight test performed in presence of atmospheric turbulence. This is done in three steps. First the output responses of a wing with the fixed shaker mass attached is obtained in clear air conditions. Then, a continuous gust excitation is applied to it resembling the atmospheric turbulence. Finally, assuming that the system is linear, the output responses of to the structure in clear air is added to that obtained due to the gust excitation. This is analyzed for the phase cross-over frequencies and the Δm values.

The analysis is performed like Section 4.7 but with a 300 grams mass ($P_f = 0.3$) instead of $P_f = 0.4$ in the earlier case, to simulate an actual flight with 300 grams added, which has been shown to be sufficient in the Section 4.5. Δm and ω_{co} vs. air velocity are shown in Figure 35. These results are very similar to those presented in Figure 34 for $P_f = 0.4$. This is expected since there are no structural or aerodynamic changes in the two cases, except that the singularity of Eq. (7) is now at about 33m/s, when Δm crosses the 0.3 line.

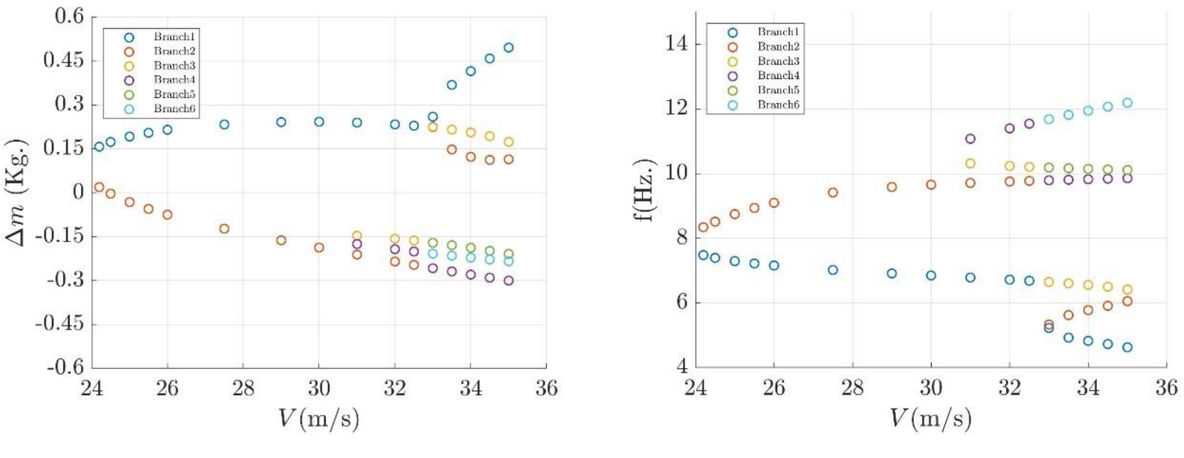

Figure 35: Δm and phase-cross-over frequencies for Pf=0.3 Kg

The effects of air turbulence are investigated below at *V*=30m/s, which is now a stable point. The gains and phases of the response due to a unit input are also shown in Figure 36. The gain plot indicates two aeroelastic frequencies at about 6 and 7 Hz., that relate to the coupled bending and torsion modes that get closer with increased velocity. The phase plot indicates two cross-over frequencies at 6.85 Hz. and 9.66 Hz. The gains at these values ($y_f(\omega_{co})$) are 17.47 m/s^2 and 2.05 m/s^2, respectively. These points correspond to the

Δm and f points at V=30m/s in Figure 35, with the one at 6.85 Hz. reflecting the critical flutter margin.

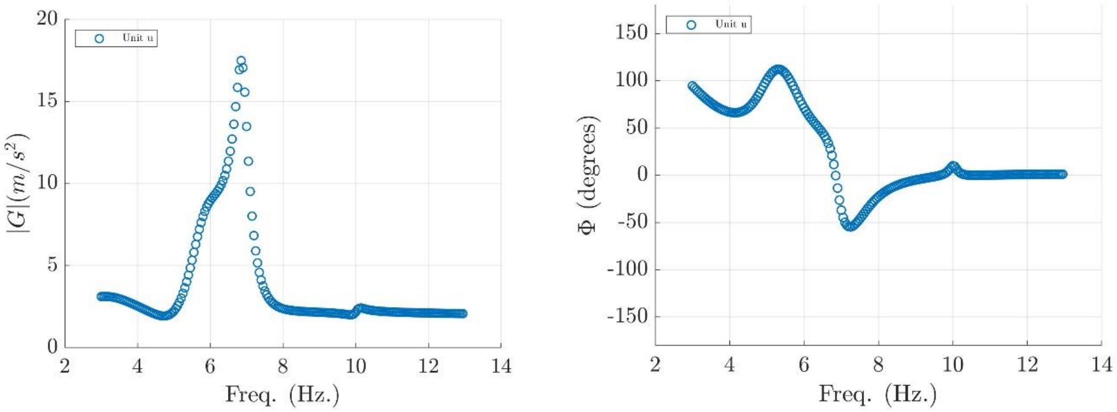

Figure 36: Gain and phase of the response due to a unit sinusoidal input, *V*=30m/s, no noise

Before adding turbulence noise to the excitation response of Figure36, the response of the system to an input signal of von-Karman's PSD with an upward induced gust velocity of 5 ft/s was obtained using Dynresp. This is probably larger than a calm test day, but the linear output response can be normalized later. The absolute response and phase of the output response is with frequency is shown in Figure 37. It can be observed that the structural response peaks are like the ones on Figure 36. The high response at low frequencies is due to the atmospheric turbulence characteristics. The total disorder of the phase plot in Figure 37 is due to the random phase associated with the gust excitation signals in Dynresp.

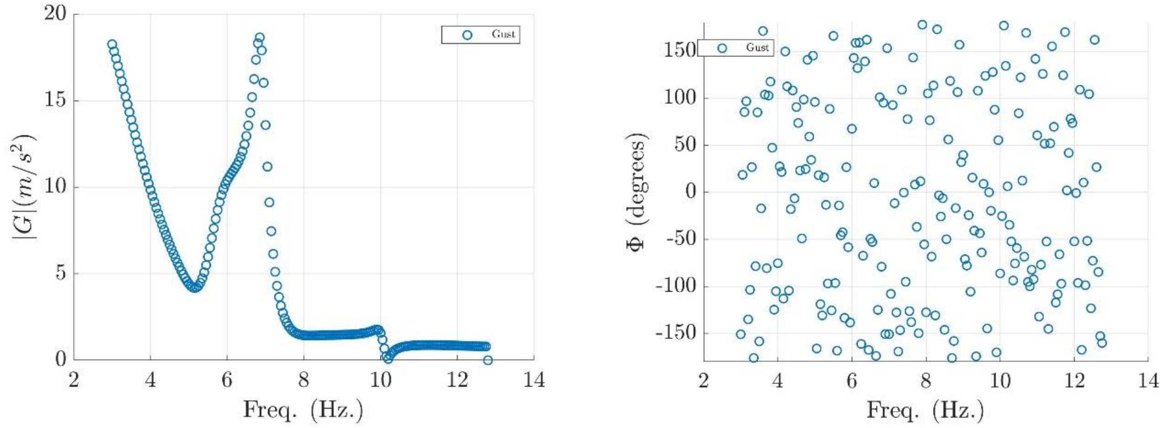

Figure 37: Gain and phase of the response due to 5 ft/s gust input

In order to analyze the system stability in presence of atmospheric turbulence, the system responses, y_g, due to the von-Karman PSD input, Figure 37, were scaled down by a normalization factor N and added to the system response, y_s, due to the unit sinusoidal input in Figure 36. Thus, the modified system response, y_m can be written as,

$$y_m = y_s + \mathrm{N}y_g \tag{13}$$

A normalization factor N=0.1 was selected here, which is expected to resemble the turbulence on a calm day. The gain and phase of y_m are shown in Figure 38, for a frequency range of 3-12.8 Hz. From the gain plot one can still see the two fundamental aeroelastic frequencies. From the phase plot, one cross-over is observed at 6.86 Hz., which is practically identical to the ideal one in Figure 35. The second phase cross-over of the modified system response is difficult to detect because of several fluctuations near zero phase around 10 Hz. However, this is not the critical flutter mechanism we need to follow in flight tests. The Δm value extracted from Figure 38 at ω_{co}=6.68 Hz. is about 0.24 Kg, which is very close to the positive Δm value at V=30m/s in Figure 35.

It may be concluded that, even though the gust excitation added significant fluctuation to the system, the main flutter margins could still be extracted with an adequate accuracy. This of course is yet to be verified in flight tests.

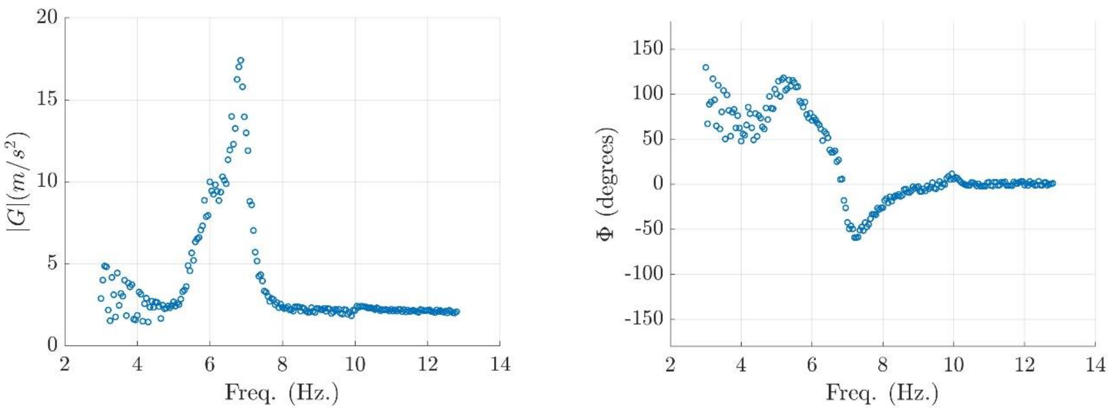

Figure 38: Gain and phase of the modified system response, 0.3Kg, with noise

5. Preliminary shaker selection

The preliminary voice-coil shaker of Figure 39, which may be adequate for the frequency range of 5-15Hz with resulting force of ~2,5N, was selected by OSU based on our preliminary specifications. The overall height is ~2.75”, and 1” in diameter: http://www.moticont.com/HVCM-025-038-003-02.htm. The moving mass is 98g and the coil is 35g, including an accelerometer in each part, for the total weight of 133g. The design currently has 1 accelerometer on the moving mass, and one on the boom attached to the wing.

Figure 39: Voice-coil shaker

A driver and closed-loop controller to provide excitation, resulting in the theoretical response curves for the moving mass at 12 Hz shown in Figure 40, was designed. By changing the position and frequency commands, a constant resultant force which is independent of excitation frequency (constant power spectra) can be designed. The housing was designed to support the shaker and allow us to reposition it along the chord of the wing. The assembly in the tip pod is depicted in Figure 41.

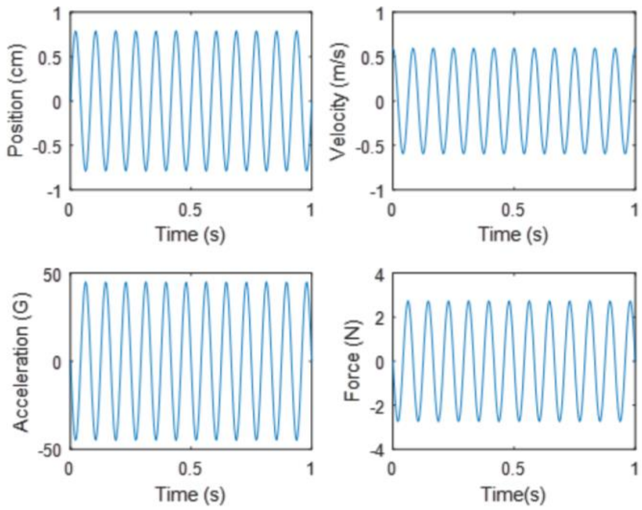

Figure 40: Acceleration and position response to 12 Hz excitation

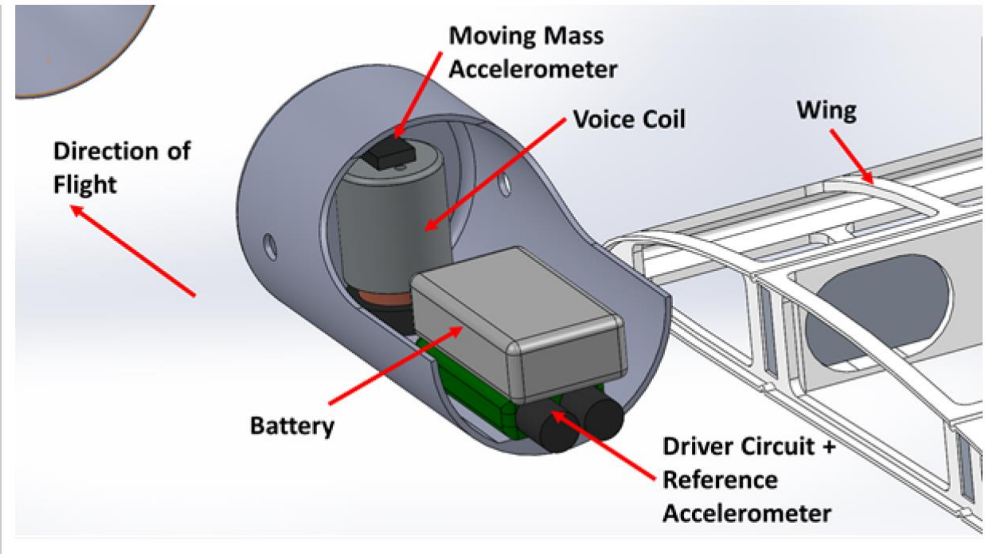

Figure 41: Preliminary shaker location in the tip tip pod

6. Flight-test conceptual plan

The logics of the planned flutter flight tests will follow those of the PFM flutter analysis in the previous section. Voice-coil shakers will be symmetrically installed at forward locations in the wing-tip pod, near Point 1 in Figure 27. The masses of the shakers itself will serve as the flutter parameter P_f. The effects of the added masses and the excitation forces to the other directions are assumed to be negligible. The added mass at forward location increases the flutter velocity, such that the flights up to the nominal flutter velocity, and beyond, will be safe. If we will find that the nominal flutter velocity is not in the available velocity range, we will reduce it by adding masses at rear locations of the tip pods.

The tip-pod shakers is being designed to provide adequate sinusoidal excitation levels in the range of 5 to 12 Hz. Accelerometers will be installed to extract the excitation forces and the resulting accelerations in the Z direction. The shakers will be synchronized to produce either symmetric or anti-symmetric excitations. Alternatively, addition and subtraction of the tip signals will provide the respective symmetric and anti-symmetric signals, allowing separate respective PFM investigations. The possibility of using one shaker only, which may reduce the test cost and/or increase safety, will also be investigated.

The flight tests will be conducted by performeing straight and level constant-velocity exercises with sinusoidal excitation sweeps. Fast Fourier Taransforms (FFT) of the filtered signals will facilitate the extcaction of the refequency-response plots, as in Fig. 15 above, and the resulting PFM plots, as in Fig. 16. Crossing the PFM=0dB point will indicate that we crossed the flutter onset velocity of the nominal vehicle (without the shaker masses). Alternatively, FRF plots as in Figure 36 will be generated and Δm and frequency plots will be extracted as in Figure 35.

The test can be stopped at this point, after recording the deformation sensors located over the aircraft (combinations of fiber optics and accelerometers) for extracting the flutter mode shapes. Obviously, the Bode and PFM plots will not be as smooth as in Figs. 15 and 16, but noisier such as in Figure 38. Signal processing for facilitating adequate evaluation of the flutter characteristics, keeping high safety levels, will be a major challenge.

7. Conclusions

1. The results of the proof-of-concept wind-tunnel tests were found to be very encouraging, forming sound baseline procedure for the current research.
2. The PFM method formulation was adapted to experimental application and has been demonstrated to yield a promising test procedure that will positively identify approached flutter conditions in a safe manner.
3. The main experimental device yet to be demonstrated in actual PFM test is an on-board shaker to be installed such that it increases the flutter velocity and used to identify the nominal flutter conditions, as demonstrated in the ideal test simulation, and the one contaminated by air turbulence, as presented in this report.

References

[1] Roizner, F., and Karpel, M., “Parametric Flutter Margin Method for Aeroservoelastic Stability Analysis”, *AIAA Journal*, Vol. 56, No. 3, 2018, pp. 1011-1022.

[2] Roizner, F. and Karpel, M., "Sensitivity of Aeroservoelastic Stability Characteristics Using Parametric Flutter Margins," *Journal of Aircraft*, Vol. 56, No. 4, July-August 2019, pp. 1387-1397, doi: 10.2514/1.C035286.

[3] M. Karpel and F. Roizner, “Towards Flutter-Boundary Tests with Controlled Vibration Levels”, proceedings of the 57th IACAS Conference, Tel Aviv, Israel, 2017.

[4] Sodja, J., Roizner, F., De Breuker, R., and Karpel, M., “Experimental Characterisation of Flutter and Divergence of 2D wing Section with Stabilized Response,” ELSEVIER Journal of Aerospace Science and Technology, No. 78, 2018, pp.542-552.

[5] Roizner, F., Raveh, D. E. and Karpel, M., "Safe Flutter Tests Using Parametric Flutter Margins," *Journal of Aircraft*, Vol. 56, No. 1, 2019, pp.228-238, doi: 10.2514/1.C035045.

[6] Sharki, B., Cesnik, C. E., Yrchieli, N., Mallik, W., Raveh, D., and Karpel, M., “Aeroelastic Analyses of the Free Flight of the Active AeroelasticAircraft Testbed (A3TB) Platform,” AIAA Paper 2021-0905, cpoceedings of the 2021 AIAA SciTech Forum, January 2021.

[7] Rodden,W. P., Harder,R. L., and Bellinger, E. D., “Aeroelastic Addition to NASTRAN,” NASA CR 3094, 1979.

[8] Ogata, K., *Modern Control Engineering*, 4th ed., Prentice-Hall, Upper Saddle River, NJ, USA, 2002.

[9] Tsiif, J., Mayer, A., Edry-Azulay, L. and Raveh, D. E., “Design, Analysis, and Testing of the Active Aeroelastic Aircraft Testbed (A3TB) Platform,” AIAA 2021-1390, SciTech 2021 Forum, January 2021.